Published in final edited form as:

Neuron. 2022 February 02; 110(3): 486–501.e7. doi:10.1016/j.neuron.2021.11.013.

Neural activity in the mouse claustrum in a cross-modal sensory selection task

Maxime Chevée[1,2,‡,&], **Eric A. Finkel**[1,‡], **Su-Jeong Kim**[1], **Daniel H. O'Connor**[1,3,4], **Solange P. Brown**[1,3,5,*]

[1]Solomon H. Snyder Department of Neuroscience, Johns Hopkins University School of Medicine, Baltimore, Maryland, 21205, USA.

[2]Biochemistry, Cellular and Molecular Biology Graduate Program, Johns Hopkins University School of Medicine, Baltimore, Maryland, 21205, USA.

[3]Kavli Neuroscience Discovery Institute, Johns Hopkins University School of Medicine, Baltimore, Maryland, 21205, USA.

[4]Brain Science Institute, Johns Hopkins University School of Medicine, Baltimore, Maryland, 21205, USA.

[5]Lead contact

SUMMARY

The claustrum, a subcortical nucleus forming extensive connections with the neocortex, has been implicated in sensory selection. Sensory-evoked claustrum activity is thought to modulate the neocortex's context-dependent response to sensory input. Recording from claustrum neurons while mice performed a tactile-visual sensory-selection task, we found that neurons in anterior claustrum, including putative optotagged claustrocortical neurons projecting to primary somatosensory cortex (S1), were rarely modulated by sensory input. Rather, they exhibited different types of direction-tuned motor responses. Furthermore, we found that claustrum neurons encoded upcoming movement during intertrial intervals and that pairs of claustrum neurons exhibiting synchronous firing were enriched for pairs preferring contralateral lick directions, suggesting that the activity of specific ensembles of similarly tuned claustrum neurons may modulate cortical activity. Chemogenetic inhibition of claustrocortical neurons decreased lick responses to inappropriate sensory stimuli. Together, our data indicate that the claustrum is integrated into higher-order premotor circuits recently implicated in decision-making.

[*]Correspondence: spbrown@jhmi.edu.
[&]Current address: Department of Pharmacology, Vanderbilt University, Nashville, TN, 37232, USA
[‡]These authors contributed equally.

Author contributions: MC, EAF, DHO and SPB designed the study. EAF and DHO developed the behavioral task. MC and EAF performed the *in vivo* experiments. MC and SJK performed anatomical experiments. MC analyzed the data with input from SPB and DHO. DHO and SPB supervised the work and acquired funding. MC and SPB wrote the original draft, which was revised by MC, EAF, SJK, DHO and SPB.

Declaration of interests: The authors declare no competing interests.

eTOC Blurb:

Chevée, Finkel et al. show that the activity of neurons in the anterior claustrum recorded during a cross-modal sensory selection task reflects movement rather than sensory input. Premotor activity in individual claustrum neurons was biased for ipsilateral or contralateral movements and encoded upcoming lick direction during intertrial intervals.

Graphical Abstract

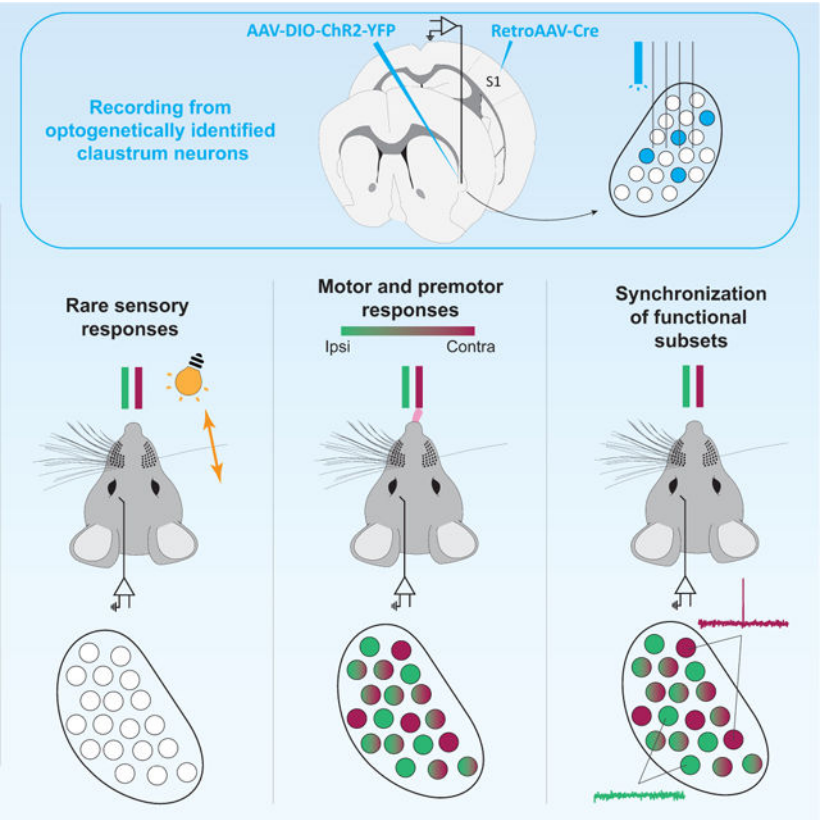

INTRODUCTION

While our brains receive a continuous barrage of sensory inputs, we must select behaviorally relevant stimuli to direct our actions. The claustrum, a small nucleus located between the insula and striatum, has been postulated to play a role in top-down control of cortical responses to sensory input (Atlan et al., 2018; Brown et al., 2017; Crick and Koch, 2005; Goll et al., 2015; Jackson et al., 2020; Smith et al., 2019; Smythies et al., 2012; White and Mathur, 2018a, b). Several experimental results indirectly support this hypothesis. First, anatomical studies show that the claustrum is highly interconnected with the neocortex, including sensory areas (Atlan et al., 2017; Clascá et al., 1992; LeVay and Sherk, 1981a; Macchi et al., 1981; Marriott et al., 2021; Wang et al., 2017; Zingg et al., 2018; Zingg et al., 2014). Reciprocal connections between the claustrum and frontal cortex are particularly prominent (Atlan et al., 2017; Tanné-Gariépy et al., 2002; Torgerson et al., 2015; Wang et al., 2017; White et al., 2017; Zingg et al., 2018; Zingg et al., 2014), providing a substrate for

signals from frontal cortex to select or suppress cortical sensory responses via the claustrum. Second, recordings of claustrum neurons have primarily shown sensory responses (Clarey and Irvine, 1986; Olson and Graybiel, 1980; Remedios et al., 2010; Remedios et al., 2014; Sherk and LeVay, 1981, but see Jankowski and O'Mara, 2015; Shima et al., 1996). Third, in tasks involving sensory distractors or high cognitive loads, behavior is compromised when claustrum activity is modulated (Atlan et al., 2018; White et al., 2020; White et al., 2018). Fourth, evidence that claustrocortical (ClaC) input suppresses cortical activity (Cortimiglia et al., 1991; Cortimiglia et al., 1987; Crescimanno et al., 1989, 1990; Crescimanno et al., 1984; Jackson et al., 2018; Liu et al., 2019; Narikiyo et al., 2020; Ptito and Lassonde, 1981; Salerno et al., 1989; Salerno et al., 1984; Tsumoto and Suda, 1982) suggests that sensory-evoked activation of claustrum neurons directly inhibits distracting cortical sensory responses. Alternative mechanisms have been proposed including that synchronous activity among functionally related subsets of ClaC neurons modulates neurons within a sensory cortical area or coordinates synchronization across cortical regions (Smythies et al., 2012, 2014; Vidyasagar and Levichkina, 2019). Although the mechanisms are different, these hypotheses all predict that the sensory responses of claustrum neurons are modulated by behavioral context.

To determine whether behavioral context modulates claustrum activity, we recorded from 545 neurons in the anterior claustrum of head-fixed mice performing a task that required animals to ignore a sensory stimulus while responding to another with distinct actions. We found that claustrum neurons, including ClaC neurons putatively projecting to S1, rarely responded to tactile or visual stimuli in this task. However, the neurons were tuned to lick direction, coded for actions both during the task and the intertrial intervals, and influenced the rate of lick responses to inappropriate sensory stimuli. Furthermore, pairs of claustrum neurons exhibiting synchronous firing were enriched for neurons preferring contralateral licks. These results indicate that anterior claustrum is integrated into higher-order premotor cortical circuits involved in perceptual decision-making (Brooks and Cullen, 2019; Guo et al., 2017; Le Merre et al., 2018; Li et al., 2016; Manita et al., 2015; Minamisawa et al., 2018; Petreanu et al., 2012; Sippy et al., 2015; Steinmetz and Moore, 2010; Svoboda and Li, 2018; Wu et al., 2020), influencing the behavioral output of mice.

RESULTS

Behavior and recording strategy

To test whether claustrum neurons respond to unattended or distracting stimuli, we trained mice to distinguish two action contexts. Head-fixed mice were presented either whisker or visual stimuli, randomly interleaved across trials. In alternating blocks (~80 trials), animals were rewarded for licking a lick port contralateral to the recording site in response to whisker deflections while ignoring visual stimuli (Respond-to-Touch Blocks), or an ipsilateral lick port in response to flashes of light while ignoring touch stimuli (Respond-to-Light Blocks; Figure 1A). Another set of mice was trained on the reversed contingencies: tactile stimulus→lick ipsilateral, visual stimulus→lick contralateral. These rules result in four trial types per block: Hit, Correct Rejection (CR), False Alarm (FA), and Miss (Figure 1A). FAs represent two error types, one where mice lick the correct port for that block

but in response to the incorrect sensory stimulus (Impulsive FAs) and one where mice lick the incorrect port for that block (Associative FAs). Respond-to-Touch and Respond-to-Light blocks were distinguishable only by the stimulus-reward contingency. Animals performing 65% of trials correctly for two consecutive days were considered trained, achieving this performance in 13–31 days (median: 16 days, Figure 1B,C).

To record the activity of claustrum neurons, we used bundles of 8 tetrodes tethered to an optic fiber and developed several strategies to confirm the location of the tetrodes within the claustrum. First, we used optogenetic tagging of ClaC neurons to confirm our electrode placement (Boyden et al., 2005; Cohen et al., 2012). We injected retro-AAV-Cre (Tervo et al., 2016) into whisker-associated S1 and AAV-DIO-ChR2-YFP into claustrum to drive Cre-dependent expression of Channelrhodopsin-2-YFP (ChR2-YFP) in putative S1-projecting ClaC neurons (Figure 1D–F, S1A). Responses to laser activation of ClaC neurons expressing ChR2 confirmed the location of our tetrodes (Figure 1G, S1B–F). Second, we coated the tetrodes with fluorescent dye and identified the tracks traversing the claustrum (Figure 1E). Third, we determined the final location of the electrode tips with electrolytic lesions (Figure 1E). Finally, we compared the electrode tracks, electrolytic lesions and ChR2-YFP ClaC neurons with the plexus of parvalbumin-positive fibers typical of the claustrum (Figure S1G–N, Druga et al., 1993; Hinova-Palova et al., 2007; Kim et al., 2016; Mathur et al., 2009; Rahman and Baizer, 2007). Using these approaches, we recorded from 247 claustrum neurons in six mice performing the task with tactile stimulus→lick contralateral and visual stimulus→lick ipsilateral reward contingencies and 298 claustrum neurons in three mice performing the reversed contingency task.

Few neurons in anterior claustrum are activated by sensory stimuli alone

The activity of claustrum neurons was clearly modulated by the task (Figure 2A,B, S2A,B,F). Many neurons increased their firing rates during Touch-Hit trials and Vision-Hit trials, but a substantial fraction were suppressed. Responses typically started after the onset of the sensory stimulus, as seen in the stimulus-aligned heatmaps of the normalized responses (Figure 2B, S2F), but largely before the first lick, as seen in the lick-aligned heatmaps (Figure S2B,S2F). Many neurons also responded during FA trials (Figure 2B, S2B).

Previous work showed that S1-projecting and V1-projecting ClaC neurons are largely distinct populations (Marriott et al., 2021). As claustrum activation inhibits cortical activity (Jackson et al., 2020) and is proposed to suppress cortical responses to distractor stimuli (Atlan et al., 2018; White et al., 2020; White et al., 2018), we hypothesized that S1-projecting ClaC neurons would be most active following tactile stimuli during Respond-to-Light blocks (Tactile stim CR trials), when animals ignore tactile stimuli, and S1 neuron responses to tactile stimuli are suppressed (Figure S2C). We recorded from 73 optotagged, putative S1-projecting ClaC neurons, representing 13.4% of the claustrum neurons we recorded (Figure S2D,E, n = 73 of 545 neurons). In contrast to our prediction, only 2 of these 73 optotagged neurons significantly responded during Tactile stim CR trials, when animals are presented a tactile stimulus but do not respond. Similarly, few responded during Visual stim CR trials in Respond-to-Touch blocks (n = 4 of 73 neurons). These results

generalized to all recorded claustrum neurons, as fewer than 5% responded significantly to the presentation of a sensory stimulus alone during CR trials, when animals withhold responses to the stimulus based on the task contingencies (Figure 2C–F). These results contrast with S1 neurons recorded under the same conditions when significantly more neurons exhibit fast, transient responses to whisker deflection during CR trials (S1 neurons responsive to touch stimuli: n = 143/754, 19.0%, S1 neurons responsive to visual stimuli: n = 4/754, 0.5%).

To further test whether individual claustrum neurons encode sensory information, we performed an ideal observer analysis by computing the ability of each neuron to discriminate between tactile stimuli occurring in Respond-to-Light blocks (Tactile stim CR trials) and visual stimuli occurring in Respond-to-Touch blocks (Visual stim CR trials), conditions under which the sensory stimuli are different and there is no motor output. Few neurons distinguished these two types of trials (n = 34 of 545 neurons). These findings are inconsistent with the hypothesis that neurons in the anterior claustrum exhibit activity triggered by distracting sensory stimuli during CR trials and directly mediate the suppression of cortical responses to sensory distractors in our task.

Claustrum neurons are recruited by movement

In contrast to the small number of neurons exhibiting sensory responses during CR trials, 77% of recorded neurons (n = 418/545) were significantly modulated during Hit trials, when the mouse licked the correct port in response to the correct sensory stimulus (Figure 3A–D). To identify which task parameters recruited claustrum neurons, we used linear discriminant analyses (LDA, n = 73 behavioral sessions, 9 mice) to ask whether sensory stimulus modality (tactile or visual, Figure 3E,H), block type (Respond-to-Touch or Respond-to-Light, Figure 3F,H) or response type (lick or no lick, Figure 3G,H) maximized the separation of claustrum neuron responses during the task. Using the 1 second following sensory stimulus onset to classify trials, regardless if a Hit, CR, FA or Miss trial resulted, we found that sensory stimulus type resulted in the lowest classification accuracy (Figure 3E,H). When block type was used to classify trials, the classification accuracy improved (Figure 3F,H). However, using the presence or absence of a lick response to classify trials, regardless of the sensory stimulus presented or the block type, maximized trial separation (Figure 3G,H). Although classifying trials based on the motor output of the mouse resulted in the greatest separation of claustrum responses, we observed that the activity of many neurons started before the mouse's first lick (Figure 2A,B, S2A,B,F).

We next compared the two types of lick trials, Hits and FAs. In both cases, mice lick, but in FA trials, they do not receive a reward. The mean firing rate was slightly higher during Hit than FA trials (Figure S3A). One possibility is that this difference reflects differences in the number of licks produced during the two trial types (Hit trials: 7.2 ± 0.02 (SEM) licks per response, n = 71,454 trials; FA trials: 6.1 ± 0.04 licks per responses, n = 24,521 trials, p = 3.0e-244, Mann-Whitney U test). However, for most neurons, there was no significant correlation between the number of licks in a response bout and their firing rate. Even among the few neurons that individually showed a significant correlation between firing rate and lick number, the relationships were not consistent across the population. For example, for the

subset of Touch-Hit responsive neurons for which the firing rate was significantly correlated with the number of licks in the response bouts (22%, n = 75 of 347 Tactile Hit-responsive neurons), the correlations were both positive and negative (60 neurons activated during licking, with 25 positively and 35 negatively correlated with the number of licks; 15 neurons inhibited during licking, with 7 positively and 8 negatively correlated with the number of licks). A second possibility is that the presence or absence of reward contributed to differences in firing rate between Hit and FA trials. However, these differences were present prior to the animal's first lick (Tactile Hit-activated neurons: Hits: 15.5 ± 0.93 spikes/s, FAs: 13.3 ± 0.82 spikes/s, n = 260 neurons, p = 2.6e-15, Wilcoxon rank-sum test; Tactile Hit-inhibited neurons: Hits: 4.6 ± 0.53 spikes/s, FAs: 5.4 ± 0.59 spikes/s, n = 87 neurons, p = 4.6e-4, Wilcoxon rank-sum test), indicating that harvesting the reward itself is not solely responsible for the differences in firing rate.

Because motor-related activity suppresses cortical sensory responses in specific contexts (Brooks and Cullen, 2019; Schneider et al., 2018), we reasoned that movement-related claustrum activity could play a role in mediating inhibition of cortical responses to sensory distractors. The activity of S1-projecting ClaC neurons may be selectively enhanced during visual stimulus-associated movement in Respond-to-Light blocks, when the mouse is suppressing tactile responses in the task (Figure 3I). If so, we would predict that activity in S1-projecting ClaC neurons is higher during Respond-to-Light lick trials (Visual Hit trials), when the mouse is suppressing tactile responses, then during Respond-to-Touch lick trials (Tactile Hit trials), when the mouse responds to tactile stimuli. We used two distinct approaches to test this hypothesis. First, we compared the mean firing rate of putative S1-projecting ClaC neurons during the 1 second following stimulus onset in Tactile and Visual Hit trials. We did not find a significant difference in firing rates across the two conditions (Figure S3B), indicating that the activity of putative S1-projecting ClaC neurons is not enhanced during Visual Hit trials. When we compared the responses across all recorded claustrum neurons, the results were similar (Figure S3C). Second, we tested whether individual putative S1-projecting ClaC neurons were better detectors of visual stimulus-associated licks than tactile stimulus-associated licks by comparing how well the single-trial activity of each predicted a tactile stimulus-associated lick versus no lick or a visual stimulus-associated lick versus no lick (Detect probability, DP; Nienborg et al., 2012). Although the DP of some neurons was strongly biased, on average, the population of putative S1-projecting ClaC neurons coded equally strongly for tactile stimulus-associated licks and visual stimulus-associated licks (Figure 3J,K). When we analyzed the DPs of putative S1-projecting ClaC neurons separately from the two cohorts of mice trained on opposite lick contingencies, the results were similar (Figure S3D,E). Similarly, when we analyzed the population of all recorded claustrum neurons, we found that it did not exhibit a systematic bias for detecting tactile or visual stimulus-associated licks (Figure S3F). As in S1 during the same task, the DP onset of responsive claustrum neurons was significantly faster for touch-associated than vision-associated licks (Figure S3G). These differences were not explained by faster reaction times to tactile relative to visual stimuli (Figure S3H). Our results indicate that the responses of both the population of putative S1-projecting ClaC neurons and of claustrum neurons more generally are not biased with respect to which

stimulus modality triggered a lick and are unlikely to directly mediate sensory-evoked inhibition of somatosensory cortex.

Claustrum neurons encode lick direction

Another possibility is that claustrum activity is biased overall for detection-associated contralateral movement, which would enable the suppression of cortical areas associated with movement to the non-rewarded side (Figure 4A). Alternatively, movement related claustrum activity may reflect a general movement signal, as seen across cortex (Musall et al., 2019; Salkoff et al., 2020; Stringer et al., 2019). To test these possibilities, we plotted the DP for lick versus no lick separately for each lick direction rather than for each sensory modality. There was no significant bias in the population preference for detection-associated contralateral versus ipsilateral licks (Figure 4B,C). These results indicate that, in the context of this task, the responses of the population of claustrum neurons are not significantly biased for contralateral licks, but do not rule out the possibility that individual neurons in the claustrum code for either contralateral or ipsilateral lick directions (Figure 4D), allowing ensembles of claustrum neurons with distinct lick direction biases to modulate targeted cortical networks depending on behavioral context.

The claustrum is reciprocally connected with frontal cortex (Atlan et al., 2017; Clascá et al., 1992; Tanné-Gariépy et al., 2002; Torgerson et al., 2015; Wang et al., 2017; White et al., 2017; Zingg et al., 2018; Zingg et al., 2014), including with premotor areas such as the anterior lateral motor cortex (ALM; Figure S4A–J; Marriott et al., 2021), where neurons selective for either ipsilateral or contralateral lick direction are intermingled (Chen et al., 2017; Guo et al., 2014; Komiyama et al., 2010; Li et al., 2015). We reasoned that if the responses of individual claustrum neurons during the task reflect consistent biases for lick direction, their direction preference during spontaneous licks, uncoupled from a stimulus response, should predict their response preferences during the task. On the other hand, if the lick direction preferences of claustrum neurons during spontaneous and detection-associated licks are uncorrelated, it would suggest that the responses reflect other features of the behavior. As with task-evoked licks, firing rates across the population of claustrum neurons showed no significant bias in preferences for spontaneous contralateral versus ipsilateral licks (Figure 4E–G, S5A). However, the onset of neural activity was faster for contralateral licks than for ipsilateral licks (Figure S5B,C), indicating that, while the average firing rate of claustrum neurons during spontaneous licks was not lateralized, the average timing of the responses was.

To further define the relationship between the lick-direction preferences of individual claustrum neurons during spontaneous versus task-evoked licks, we took two independent approaches. First, we computed the correlation between each neuron’s lick direction preferences determined using spontaneous and detection-associated licks. We found that these values were strongly correlated, both for optotagged, putative S1-projecting ClaC neurons ($r = 0.91$, $n = 73$ neurons) and the population of all recorded claustrum neurons (Figure 4H, $r = 0.85$, $n = 545$ neurons). Second, we calculated the direction preferences of individual neurons based on their spontaneous lick-direction preference and used these preferences to decode, on a trial-by-trial basis, whether a mouse licked contralaterally or

ipsilaterally during the task (Mayrhofer et al., 2019). This strategy successfully decoded the animal's choice during the task (Figure 4I), indicating that a claustrum neuron's lick direction preference is similar during spontaneous and task-evoked licks. Our analyses show that individual claustrum neurons exhibit lick direction preferences, and that claustrum activity during behavioral trials reflects these preferences.

The claustrum is enriched for synchronous spiking between neurons preferring contralateral licks

Several studies hypothesize that synchronous activity among claustrum neurons influences cortical activity by modulating the activity of local groups of related cortical neurons or potentiating synchronization across cortical regions (Smythies et al., 2012, 2014; Vidyasagar and Levichkina, 2019). A recent study found that the local circuit organization of the claustrum is consistent with a neural circuit that promotes synchronized activity among its neurons (Kim et al., 2016). Because we found that neurons in the anterior claustrum encode lick direction, we reasoned that, if these correlations coordinate the activity of cortical neurons engaged in the task, pairs of neurons with similar lick direction preferences should be more correlated than pairs with opposite lick direction preferences. Therefore, we tested for correlated activity between simultaneously recorded neurons in the claustrum and asked whether these neurons shared tuning properties. We computed the cross-correlogram (CCG) during the inter-trial interval, using the 1 second prior to sensory stimulus onset, for all pairs of claustrum neurons recorded simultaneously on different tetrodes (n = 1924 pairs). Although most pairs were not correlated, we identified pairs exhibiting correlations at short, millisecond timescales (Figure 5A,B). A greater proportion of pairs of claustrum neurons was significantly correlated than pairs of S1 neurons recorded with tetrodes under similar conditions, though the difference was modest (Figure 5C). This difference remained when the analysis was performed during the 1 second following sensory stimulus onset (Figure S6A). The percent of pairs exhibiting correlations prior to stimulus onset did not change with block type (Respond-to-Touch Blocks: 2.9%, n = 55/1924 pairs; Respond-to-Light Blocks: 3.0%, n = 58/1924 pairs, Chi square p = 0.85) or with correct or incorrect response type (Correct trials (Hit and CR): 3.3%; n = 65/1924 pairs; Incorrect trials (Miss and FA): 2.5%, n = 48/1924 pairs, Chi Square, p = 0.13). We also found that the correlations in the claustrum were stronger than those recorded in S1 (Figure 5D, S6B) and that the timing differed: the widths of the cross-correlograms were significantly narrower for pairs of claustrum neurons than for pairs of S1 neurons (Figure S6C–H). These differences were not explained by firing rates alone, as we normalized CCGs by the geometric mean firing rates. Furthermore, the mean firing rates were higher in S1 than in the claustrum in the 1 second prior to stimulus onset (Neurons in all pairs: S1: 8.92 ± 0.27 Hz (SEM), n = 656 S1 neurons; Claustrum: 6.29 ± 0.30 Hz, n = 491 claustrum neurons, p = 1.29e-16, Mann-Whitney U test; Neurons in correlated pairs: S1: 11.35 ± 0.76 Hz, n = 141 S1 neurons; Claustrum: 9.31 ± 0.82 Hz, n = 112 claustrum neurons, p = 0.00984, Mann-Whitney U test), which would if anything artificially strengthen correlations among S1 neurons, the opposite of what we observed.

To further test our hypothesis that pairs with similar lick direction tuning are more correlated than pairs with opposite lick direction preferences, we plotted a lick direction preference

index for all recorded pairs (Figure 5E) and compared the proportions of significantly correlated pairs for each possible combination of preferences: contra-contra, ipsi-ipsi or contra-ipsi. As predicted, neuron pairs with fast timescale correlations were significantly enriched for pairs preferring the same lick direction (Figure 5F). Unexpectedly, significantly correlated pairs were enriched for pairs in which both neurons preferred contralateral licks (Figure 5F). The strength of the correlations among claustrum neurons preferring contralateral licks, however, did not depend on the lick direction rewarded during that block (Contralateral lick blocks: 10.5 ± 2.9 % coincident spikes; Ipsilateral lick blocks: 9.7 ± 2.9 % coincident spikes; n = 20 contralaterally tuned pairs; p = 0.79, Wilcoxon signed-rank test). Therefore, while the lick-direction preference of the population of recorded claustrum neurons was not biased, with ipsilateral and contralateral lick directions equally encoded across the population, the activity of neurons preferring contralateral licks was preferentially correlated. This result further suggests subtle lateralization of claustrum function, similar to the significant difference in the onset of neural activity for contralateral versus ipsilateral spontaneous licks (Figure S5B,C). The findings regarding the prevalence, strength and timing of synchronous activity in the claustrum support the hypothesis that the circuit organization of the claustrum promotes synchronous activity among functionally related claustrum neurons and further suggest that functionally distinct subsets of claustrum neurons may influence cortex differentially through their preferential correlations.

The activity of claustrum neurons prior to stimulus presentation encodes upcoming lick direction

To visualize the variety of responses in our recordings, we clustered neurons based on their mean activity during both types of Hit trials (Tactile and Visual Hit trials; Figure S7A,B). This visualization revealed groups of neurons that were inhibited (25% of neurons, n = 134/545 neurons), activated (56%; n = 306/545 neurons) or not modulated during the task (19%, n = 105/545 neurons; Group 12). Interestingly, the non-modulated group (Group 12) was depleted for putative S1-projecting ClaC neurons (n = 7/105 neurons; p = 0.0015, Bonferroni corrected hypergeometric test). Of the 12 groups, each contained neurons recorded from six to nine mice but for Group 11 (Figure S7C). Although groups were distinguished by the envelope and time course of their responses, most groups of activated neurons exhibited similar activity during Tactile and Visual Hit trials (Figure S7A,B; Groups 1, 3, 4, 5 and 13, 44%; n = 240/545 neurons).

Four groups activated during Hit trials, however, exhibited different responses during Respond-to-Touch and Respond-to-Light Hit trials (Figure S7A,B; Groups 2, 6, 10 and 11, 12%; n = 66/545 neurons). Of those, Groups 2, 6 and 11 exhibited shifts in their baseline firing rates preceding the presentation of the sensory stimulus (Figure S7B). Because claustrum neurons encode the direction of movement, and the claustrum is interconnected with premotor areas including ALM (Figure S4; Atlan et al., 2017; Marriott et al., 2021; Smith and Alloway, 2014; Smith et al., 2012; Wang et al., 2017; White et al., 2017; Zingg et al., 2014), we hypothesized that these baseline shifts reflect persistent activity related to upcoming movement, similar to activity observed in premotor areas in rodents and the frontal eye fields in monkeys (Squire et al., 2013; Svoboda and Li, 2018). Therefore,

we tested whether claustrum activity prior to the delivery of the sensory stimulus reflects upcoming movement during Respond-to-Touch and Respond-to-Light blocks.

We analyzed the activity of strongly lick direction-preferring neurons (Figure 6A) during the 1 second preceding sensory stimulus onset, omitting trials in which the mouse contacted either spout during this period. We found that the population of claustrum neurons coded for upcoming lick direction based on their lick direction preference. The responses of two example neurons are shown: one preferring contralateral licks showing enhanced firing preceding sensory stimulus onset during blocks rewarding contralateral licks (Figure 6B-left) and one preferring ipsilateral licks exhibiting higher firing prior to sensory stimulus onset during blocks rewarding ipsilateral licks (Figure 6B-right). We analyzed the population of lick direction-preferring claustrum neurons by computing an Upcoming Lick Direction Index (ULDI) based on their activity during the 1 second preceding sensory stimulus onset. We found that the ULDI for the population of claustrum neurons preferring contralateral licks was significantly greater than zero, indicating that their prestimulus activity encoded upcoming contralateral licks, while the ULDI for claustrum neurons preferring ipsilateral licks was significantly smaller than zero, indicating their prestimulus activity encoded upcoming ipsilateral licks (Figure 6C). These results show that claustrum neurons maintain a representation of the block-type the mouse is in based on their motor tuning, activity that may allow them to influence cortical responses associated with either ipsilateral or contralateral licks in our task.

Inhibiting claustrum neurons decreases the rate of impulsive false alarms

Because our recordings revealed that claustrum neurons are activated both prior to and during licks and maintain a representation of block-type, we hypothesized that manipulating claustrum activity would influence licking movements during the task. To test this hypothesis, we bilaterally expressed the inhibitory DREADD, hM4Di-mCherry (Figure 6D, n = 6 mice), or a control mCherry virus (n = 5 mice) in ClaC neurons using a similar strategy as for expressing ChR2 in ClaC neurons (Figure 1D). However, because the responses of putative S1-projecting ClaC neurons did not differ from those of other claustrum neurons, we targeted a broader population of ClaC neurons in both hemispheres (Figure 6D, see Methods). Once animals reached the learning criterion on the cross-modal selection task, we administered the DREADD agonist or vehicle on alternating days. We first compared the Hit rate for DREADD and control mice and found it unaffected across conditions (Figure 6E). The number of inter-trial licks was also unaffected by agonist administration (mixed ANOVA with repeated measure for injection and independence for virus: interaction of virus and injection $F = 1.75$; $p = 0.218$). These results indicate that the mouse's overall ability to generate licks was unaffected by our chemogenetic manipulation. However, when we compared the effects of DREADD agonist administration on the FA rate, we found that Impulsive FAs, when mice lick the correct lick port for that block but in response to the incorrect sensory stimulus, were decreased (Figure 6F). There was no change in the rate of the rarer Associative FAs, when mice lick the wrong lick port for that block (Figure 6G). These results indicate that the rate of impulsive licks triggered by distracting stimuli are influenced by changes in claustrum activity. Together, our findings support the hypothesis that the activity of ClaC neurons preceding and during lick execution in our task

plays an important role in priming premotor circuits for the correct lick response for the block and contributes to impulsive responses triggered by the wrong stimulus.

DISCUSSION

Prior electrophysiological studies reported primarily sensory responses in the claustrum (Clarey and Irvine, 1986; LeVay and Sherk, 1981b; Olson and Graybiel, 1980; Remedios et al., 2010, but see Jankowski and O'Mara, 2015; Shima et al., 1996). Possible reasons for the discrepancy between these results and ours include the behavioral state of the animals and the location of the recordings. Previous studies largely focused on anesthetized animals or animals passively receiving sensory input rather than engaged in a task. We also likely sampled a region of claustrum more anterior than previous work. However, even putative S1-projecting ClaC neurons in anterior claustrum rarely exhibited responses to sensory stimuli alone. It remains possible that neurons in the posterior claustrum of the mouse exhibit responses evoked by sensory stimuli, and that the claustrum has specialized regions with distinct roles (Chia et al., 2020; LeVay and Sherk, 1981b; Olson and Graybiel, 1980; Remedios et al., 2010). Whether ClaC neurons in different claustral regions or targeting different cortical areas differentially contribute to hypothesized claustrum functions such as context-reward associations (Terem et al., 2020), optimal behavioral performance during high cognitive loads (White et al., 2020; White et al., 2018) and sleep (Narikiyo et al., 2020; Norimoto et al., 2020; Renouard et al., 2015) remains an important question.

Several studies hypothesize that synchronous activity among claustrum neurons influences the activity of related ensembles of cortical neurons within or across cortical areas (Smythies et al., 2012, 2014; Vidyasagar and Levichkina, 2019). That the claustrum shows more synchronous activity than S1 is consistent with the proposed circuit organization of the claustrum (Kim et al., 2016; White and Mathur, 2018b; White et al., 2018). These ensembles may be particularly effective at activating or synchronizing functionally related subsets of cortical neurons, even though pairs exhibiting synchronous activity represented a small minority of recorded pairs. Although we did not find a contralateral bias in the response selectivity of claustrum neurons, the enrichment for contralateral-preferring neurons in synchronous pairs and the faster onset of activity for contralateral licks suggests the claustrum shows some functional lateralization, perhaps reflecting that some motor and frontal cortical regions project more strongly to contralateral claustrum (Alloway et al., 2009; Wang et al., 2017).

We set out to test the hypothesis that claustrum plays a role in sensory selection similar to that performed by interactions between the prefrontal cortex and the thalamoreticular nucleus (TRN), in which top-down signals modulate the gain of cortical sensory responses (Wimmer et al., 2015). However, our results were inconsistent with a mechanism by which claustrum neurons respond to sensory input and inhibit sensory responses. Rather, the vast majority of neurons we recorded encoded signals related to movement, although a contribution of reward anticipation to the responses remains possible. A previous study in non-human primates also identified movement-related neurons in the claustrum, but the responses did not reflect specific movements or movement context (Shima et al., 1996). The responses of claustrum neurons we observed here were instead lick-direction

specific, similar to those of neurons recorded in ALM (Chabrol et al., 2019; Chen et al., 2017; Economo et al., 2018; Guo et al., 2017; Guo et al., 2014; Inagaki et al., 2019; Inagaki et al., 2018; Li et al., 2015; Li et al., 2016; Wu et al., 2020). As in motor areas (Alexander and Crutcher, 1990; Murakami et al., 2014; Riehle and Requin, 1989), claustrum neurons exhibited different temporal response profiles, including inhibition, and their baseline activity reflected the direction of upcoming licks, although we cannot entirely rule out that small tongue and jaw movements contributed to generating the premotor activity we observed (Esmaeili et al., 2021; Massion, 1992; Musall et al., 2019). Anatomical reconstructions of individual corticoclaustral neurons in premotor cortex show that they are layer 5 intratelencephalic (L5 IT) neurons, with axon branches in the striatum (Lévesque and Parent, 1998; Parent and Parent, 2006) and recent studies indicate that L5 IT neurons in ALM code equally well for both ipsilateral and contralateral intended licks (Li et al., 2015), similar to the claustrum neurons we recorded here. Because L5 IT neurons play key roles in maintaining preparatory activity in ALM (Li et al., 2016; Wu et al., 2020), reciprocal connections between claustrum and premotor areas may contribute to generating preparatory activity patterns.

When we inhibited ClaC neurons bilaterally using inhibitory DREADDs, the rate of Impulsive FAs was decreased while the Hit rate remained unchanged. As previous studies have reported that motor, premotor and frontal cortex are inhibited following activation of ClaC neurons by brief electrical or optogenetic activation (Cortimiglia et al., 1991; Cortimiglia et al., 1987; Crescimanno et al., 1989, 1990; Crescimanno et al., 1984; Jackson et al., 2018; Narikiyo et al., 2020; Salerno et al., 1989; Salerno et al., 1984), it is possible that the cortex was disinhibited by inhibition of ClaC neurons, increasing suppression of unwanted movements and resulting in a decrease in Impulsive FAs (Ebbesen and Brecht, 2017; Esmaeili et al., 2021). This interpretation would be consistent with results following inhibition of motor and frontal cortex including ALM during Go-No Go tasks, in which the rate of FAs increases without much altering the Hit rate (Goard et al., 2016; Hu et al., 2019; Huber et al., 2012; Kamigaki and Dan, 2017; Salkoff et al., 2020; Zagha et al., 2015) although inhibiting ALM impairs performance requiring lick responses under some conditions (Guo et al., 2014; Inagaki et al., 2019; Inagaki et al., 2018; Li et al., 2015; Li et al., 2016). Our results are also consistent with a prior study in which increasing claustrum activity in rats increased the rate of impulsive premature responses in a 5-choice serial reaction time task (Liu et al., 2019), although these effects may depend on task structure or on the particular type of ClaC neurons involved (Atlan et al., 2021). In addition, how ClaC inputs influence the different cell types in prefrontal and motor cortical areas with different contributions to these behaviors (Economo et al., 2018; Huber et al., 2012; Li et al., 2020; Zagha et al., 2013) remains an open question. Furthermore, as some neurons outside the canonical boundaries of the claustrum expressed DREADDs, it is possible that small populations of neurons in other brain regions contributed to the decrease in Impulsive FAs. Nonetheless, our results indicate that claustrocortical loops exhibit preparatory activity and may regulate premotor circuits involved in suppressing unwanted movements in response to inappropriate stimuli.

RESOURCE AVAILABILITY

Lead Contact—Further information and requests for resources and reagents should be directed to and will be fulfilled by the Lead Contact, Solange P. Brown (spbrown@jhmi.edu).

Materials Availability—This study did not generate new unique reagents.

Data and Code Availability

- All data and code used for analysis and figure generation are available upon request.
- Original code has also been deposited at Zenodo and is publicly available as of the date of publication. The DOI is listed in the key resources table.
- Any additional information required to reanalyze the data reported in this paper is available from the lead contact upon request.

EXPERIMENTAL MODEL AND SUBJECT DETAILS

Mice—All procedures were approved by the Johns Hopkins Animal Care and Use Committee and followed the guidelines of the Society for Neuroscience and the National Institutes of Health. Animals used for *in vivo* electrophysiology and the DREADD experiments ranged in age from 2 to 5 months during the recordings. Both males and females were used in this study (sex indicated for each replicate in methods below). All animals were kept on a 12 h light/dark cycle and provided with unlimited food and water until water restriction began (see details below). Information about the generation and genotyping of the lox-STOP-lox-tdTomato line used in this study can be found in the original studies (Ai9 and Ai14; Madisen et al., 2010). Mice were maintained on mixed backgrounds including C57BL/6J and CD-1 but were primarily C57BL/6J.

METHOD DETAILS

Stereotactic injections and microdrive implantation—To express Channelrhodopsin-2 (ChR2) in claustrocortical (ClaC) neurons projecting to the somatosensory cortex barrel field (S1BF), LSL-tdTomato mice (P35 to P127) were anesthetized with ketamine (50 mg/kg), dexmedetomidine (25 μg/kg) and the inhalation anesthetic, isoflurane. Animals were placed in a custom-built stereotactic frame and anesthesia was maintained with isoflurane (1–2.5%). The scalp and periosteum were removed, and a small craniotomy was performed above left S1. A glass pipette (10–25 μm tip diameter) was lowered into S1BF (1.1 mm posterior to Bregma, 3.1 mm lateral to Bregma, 0.5 mm from the surface of the brain) and 60–120 nL of retroAAV-Cre (rAAV2-retro-Syn-Cre, Tervo et al., 2016) or AAVrg-pmSyn1-EBFP-Cre (Addgene viral prep # 51507-AAVrg, a gift from Hongkui Zeng) were pressure-injected. The pipette was kept in position for 5–10 minutes before removal, and the craniotomy was then covered with a thin layer of Kwik-cast (World Precision Instruments). The skull was roughed using a dental drill (Athena Champion AC5000, NTI Diamond F132–008 diamond burr) and a custom-made headplate was affixed using cyanoacrylate adhesive (Krazy Glue). A ground screw was

implanted above the cerebellum and a second craniotomy was performed above the left claustrum. A glass pipette (10–25 μm tip diameter) was lowered into the left claustrum (1.7 mm anterior to Bregma, 2.7 mm lateral to Bregma, 2.65 mm from the surface of the brain) and between 180 and 270 nL of AAV5-DIO-Ef1a-hChR2(H134R)-EYFP-WPRE-hGH (Addgene viral prep #20298 or UNC Vector Core, a gift of Karl Deisseroth) were pressure injected. The pipette was kept in position for 5–10 minutes before removal. Mice were then implanted with a custom-made microdrive (8 tetrodes, Cohen et al., 2012) coupled to an optic fiber (200 μm diameter, 0.39 NA) initially targeted to a region above the claustrum (1.7 mm anterior to Bregma, 2.7 mm lateral to Bregma, 1.8 mm from the surface of the brain). The tips of the tetrodes were between 0.6 and 0.9 mm from the tip of the optic fiber, and both were coated with red retrobeads (Lumafluor) to facilitate the identification of the tetrode tracks following the electrophysiology experiments. The microdrive was secured to the headplate using cyanoacrylate gel super glue (The Original Super Glue Corporation) and dental cement (Jet Repair Acrylic Pound Package, Pearson Dental).

Similar procedures were used to express the inhibitory DREADD receptor or control fluorophore in ClaC neurons. Because the responses of putative S1-projecting ClaC neurons did not differ from those of other claustrum neurons, we targeted a broader population of ClaC neurons, injecting a retroAAV-Cre virus into S1, ALM, retrosplenial cortex (RSP), and anterior cingulate cortex (ACC) bilaterally and the DREADD or control virus into the claustrum in both hemispheres. We chose these additional cortical locations as many ClaC neurons project to these regions (Marriott et al., 2021; Wang et al., 2017).100 nL of retroAAV-hSyn-HI-eGFP-CRE-WPRE-SV40 (Addgene viral prep #105540-AAVrg, a gift from James M. Wilson) was stereotaxically injected into four locations bilaterally, for a total of 8 injections: S1BF (1.1 mm posterior to Bregma, 3.1 mm lateral to Bregma, 0.5 mm from the surface of the brain), anterior lateral motor cortex (ALM; 2.5 mm anterior to Bregma, 1.5 mm lateral to Bregma, 0.5 mm from the surface of the brain), retrosplenial cortex (RSP, 3.0 mm posterior to Bregma, 0.5 mm lateral to Bregma, 0.5 mm from the surface of the brain) and anterior cingulate cortex (ACC, 0.5 mm anterior to Bregma, 0.3 mm lateral to Bregma, 0.5 mm from the surface of the brain). Then four 100 nL injections of AAV5-hSyn-DIO-hM4D(Gi)-mCherry (Addgene viral prep #44362-AAV5, a gift from Bryan Roth) or AAV5-hSyn-DIO-mCherry (Addgene viral prep #50459-AAV5, a gift from Bryan Roth) were injected in each claustrum bilaterally along its anteroposterior axis (Injection coordinates AP/ML/DV from surface: 1.9 mm/2.6 mm/2.4 mm; 1.4 mm/2.8 mm/2.6 mm; 0.9 mm/3.2 mm/2.8 mm; 0.4 mm/3.2 mm/2.8 mm). The headplate was implanted as described above, but no microdrive was implanted.

To label corticoclaustral projections from ALM, 90 nL of AAV-DJ-CamKIIa-ChR2(H134R)-eYFP (GVVC-AAV-36, Stanford Gene Vector and Virus Core, a gift from Karl Deisseroth) was pressure injected into ALM (−2.5 mm anterior to Bregma, 1.5 mm lateral to Bregma, 0.8 mm from the surface of the brain) of 4 mice (P75-P83, 2 males and 2 females). In the same mice, 90 nL of Alexa Fluor 555-conjugated Cholera Toxin Subunit B (CTB; ThermoFisher Scientific) was injected into S1BF (1 mm posterior to Bregma, 2.8 mm or 3.1 mm lateral to Bregma, 0.8 mm from the surface of the brain) to retrogradely label S1-projecting ClaC neurons and compare their cell body locations with the location of the ALM corticoclaustral axons. Animals were sacrificed 10 days following the injections.

Buprenorphine (0.05 mg/kg) was administered to all animals postoperatively.

Behavioral task—All behavioral experiments were conducted with head-fixed mice trained in a cross-modal sensory selection task. The behavioral apparatus was controlled by BControl software (C. Brody, Princeton University) or by Arduino pro mini ATMega328p (Arduino: E000025, Sparkfun ATMega328). One week following surgery, ChR2 mice were restricted to 1 mL of water per day. During the water restriction period, mice were handled daily and head fixed in the behavioral apparatus for increasing amounts of time (starting at 5 minutes). When a mouse's weight stabilized at 80% of its pre-water restriction weight (~1 week), training was started. For mice used in the DREADD experiments, training began 28 days following the surgery. During training and experimental sessions, mice obtained water while performing the task. Supplemental water was given to maintain a body weight of 80% or greater than the pre-restriction weight. Behavioral sessions occurred once per day and lasted until the mouse stopped performing, usually ~1 hour.

Mice were first taught to lick two reward ports located 6–10 mm anterior and ~35 degrees to the left and right of the midline to collect water drops (~6 μl). Contacts between the tongue and the lick port were detected by a conductive lick detector (Svoboda lab, HHMI Janelia Research Campus), and water delivery was controlled by a solenoid valve (LHDA0531115H, The Lee Company). Mice quickly associated licking with the collection of water rewards (~1 day) and from that point, we started stimulus detection training.

During the initial training, the sensory modality, touch or vision, with which to begin training was randomly selected. To generate tactile stimuli, a single whisker (one of C1–3 or D1–3) on the right whisker pad was threaded into a glass pipette attached to a piezo actuator (D220-A4–203YB, Piezo Systems), which was driven by a piezo controller (MDTC93B, Thorlabs). Approximately 1.5 mm of whisker remained exposed at the base. At first, mice were rewarded automatically upon whisker stimulation (sinusoidal deflections at 40 Hz, 1 s, ~1400 deg/s), on the right or left lick port depending on the contingency (Respond-Right-to-Touch, n = 6 mice, 4 females and 2 males; Respond-Left-to-Touch, n = 3 mice, 2 females and 1 male). The automated reward delivery was removed after ~1–2 days, and the mice were rewarded for licking the correct port 0.1 s to 1.5 s after stimulus onset. Licks that occurred within the 0.1 s period immediately following stimulus onset were not rewarded. Licks occurring in a 0.2 s period prior to stimulus onset resulted in the withholding of the stimulus presentation for that trial and no reward or punishment. Trials with withheld stimuli were omitted from analysis. For visual detection training, a 1 s flash of 565 nm light (~50 mW) generated by an LED (M470F1 LED driven by LEDD1B, Thorlabs) and emitted from the tip of an optic fiber (105 μm diameter, 0.22 NA; M43L01, Thorlabs) positioned 5.5 cm away from the tip of the mouse's nose along its midline was used as stimulation. Mice were rewarded for licking the right (n = 3 mice) or left (n = 6 mice) port, depending on the task contingency, and trained as described above for the tactile stimulus. Once mice reliably collected water rewards for one of the two modalities (~1–4 days), we switched to training the mouse on the other modality.

In the next stage of task training, randomly interleaved stimuli were delivered (touch: 0.15 s sinusoidal deflections at 20 Hz, ~600 deg/s; vision: 0.15 s flash, ~3 mW at the tip of

the optic fiber attenuated using a neutral density filter; optical density = 3 to 6, NE530B, Thorlabs). The stimulus intensities were selected such that animals plateaued at ~70% correct trials. The inter-trial period consisted of a 3.5 s fixed interval to which a random interval drawn from an exponential distribution with a 4 s mean was added. Mice were required to respond to only one of the two modalities during blocks of trials, with the modality alternating between blocks, to receive water rewards. We trained two sets of ChR2 animals on two contingencies: during Respond-to-Touch blocks, a first set (n = 6 mice, 2 females and 4 males) was rewarded for licking the right port following a tactile stimulus and, during Respond-to-Light blocks, for licking the left port following a visual stimulus. For a second set (n = 3 mice, 2 females and 1 male), mice were rewarded for licking the left port following a tactile stimulus during Respond-to-Touch blocks and the right port following a visual stimulus during Respond-to-Light blocks. Mice used in the DREADD experiments (n = 11) were rewarded for licking the right port following a tactile stimulus during Respond-to-Touch blocks and for licking the left port following a visual stimulus during Respond-to-Light blocks. Successful execution of these rules resulted in Hit trials (when the mouse responded correctly to the rewarded pairing between sensory modality and lick spout) and Correct Rejection trials (CR, when the mouse correctly withheld its response to the non-rewarded sensory modality) for each block type. Trials during which mice responded to the incorrect, non-rewarded sensory stimulus during a block or licked the wrong lick spout were considered False Alarms (Impulsive or Associative FAs, respectively). Trials when the mice did not respond to the correct, rewarded sensory stimulus were considered Misses. Incorrect responses did not result in any punishment. Initially, blocks contained ~150 trials each to minimize the number of switches during a training session. As training progressed, the block length was lowered to ~80 trials, resulting in the reward rule alternating 3–5 times per session. At each block transition, mice were allowed ~10 trials to switch, after which we encouraged them to switch reward contingency via manual release of water at the correct reward port. The mice then typically switched immediately.

We computed the percent correct trials to assess performance: 100*(# Hits + # Correct Rejections) / (Total # of trials) and considered mice trained once they performed > 65% correct for at least two consecutive days at the stimulus intensities selected. For the remainder of the recording sessions, sessions during which overall performance was < 65% correct or < 60% correct for either block type were omitted from further analysis. Low-frame rate video recordings of trained mice showed that they make occasional small tongue or jaw movements that do not contact the lick spout during the intertrial intervals which we did not analyze further.

In vivo electrophysiology data pre-processing—Neural signals and behavioral timestamps were recorded using an Intan system (RHD2000 series multi-channel amplifier chip; Intan Technologies) at a sampling rate of 30 kHz. Recordings were bandpass filtered at 700–6,000 Hz, and the signal common to all electrodes was subtracted (common-mode rejection). Spikes were sorted offline using MClust software (A. David Redish). Only clusters with few inter-spike interval (ISI) violations (< 1% of cluster spikes within 2 ms) and a small L-ratio (indicative of cluster isolation quality, L-ratio < 0.1) were selected as putative single neurons. Clusters were also excluded if drift or unstable waveforms were

observed. In total, we recorded from 1216 neurons. Data processing was performed similarly for the tetrode recordings performed in S1.

Post hoc confirmation of tetrode location: Following the last recording session, we made electrolytic lesions to mark the location of the tetrodes. Animals were placed in a custom-built stereotactic frame and anesthesia was maintained with isoflurane (1–2.5%). 20 μA were passed through the tetrodes with which optogenetic responses were detected (see section below) for 10 s using a constant current stimulus isolator (World Precision Instruments, A365RC). Animals were sacrificed 24 h post lesion. To further visualize the trajectory of the tetrode/optic fiber bundle during the recording sessions, we coated them with red retrobeads (Lumafluor) before insertion. Only experiments with tracks marked by red retrobeads traversing the claustrum, electrolytic lesions positioned consistent with the tetrode trajectory, and optotagged ClaC neurons (see below) were kept for analysis.

Optogenetic identification of claustrum neurons—After the completion of each behavioral session, we used an optogenetic approach to identify optogenetically modulated neurons and to confirm the location of the tetrodes in the claustrum. The implanted optic fiber was coupled to a 473 nm laser (Laserglow Technologies: LRS-0473-PFM-00100–03) and trains of 3 ms pulses were delivered at 2 Hz (Power at the tip of the optic fiber: ~10 mW) using an optical shutter (Uniblitz shutter: LS2S2T1, shutter driver: VCM-D1) controlled by an Arduino (Arduino Uno R3). We used the method described in Kvitsiani et al., 2013 (SALT) to identify neurons with latencies to first spike significantly modulated following a laser pulse ($p < 0.05$ in a 10 ms window). Only neurons with a mean number of action potentials > 0.1 during the 10 ms window following the laser pulse were counted (Figure S1B, n = 142 of 1216 neurons). Detecting these neurons, which include putative ChR2-expressing, S1-projecting ClaC neurons as well as neurons possibly postsynaptic to ChR2-expressing neurons, further confirmed tetrode placement in the claustrum. Laser-responsive neurons were absent when we mistargeted the claustrum altogether as confirmed by the tetrode tracks and the location of the electrolytic lesions. By combining the *post hoc* anatomical analyses of the tetrode tracks and electrolytic lesions with the optogenetic analyses, we delineated the boundaries of the claustrum as our tetrodes traversed it in each animal. Neurons that were modulated by the laser pulses were identified as being in the claustrum. For neurons whose activity was not modulated by the laser pulses, we identified them as being located in the claustrum under two conditions. First, any neuron recorded on the same tetrode simultaneously with an optogenetically modulated neuron was defined as being in the claustrum. Second, if a neuron was recorded between a more dorsal and a more ventral location at which optogenetically modulated neurons were identified on that tetrode (see grey locations in Figure S1F), then these neurons were also defined as being within the claustrum. This definition was consistent with the relationships between the claustrum, the tetrode tracks and the electrolytic lesions we identified anatomically. This approach allowed us to determine the boundaries of the claustrum traversed by the tetrodes for each animal and to include all single units recorded within these defined boundaries in our data set of claustrum neurons (Figure S1F, n = 545 claustrum neurons). Neurons not included within these boundaries were not analyzed further.

Identification of putative S1-projecting claustrocortical neurons—We applied more strict criteria to optogenetically identify putative S1-projecting ClaC neurons directly transfected with rAAV-Cre and AAV-DIO-ChR2 (Optotagged neurons). We delivered 10 Hz trains of laser pulses and used the following criteria: 1) first spike latency: < 7 ms; 2) waveform correlation between laser-evoked spikes and spikes recorded during the behavioral session: > 0.9; and 3) probability of spike following laser pulse: > 0.3. For each pulse, the first spike occurring between 3 ms preceding and 3 ms following the mean first spike latency for each neuron was counted as laser evoked and contributed to computing the reliability of spiking. We identified 73 putatively S1-projecting ClaC neurons ("Opto-tagged"). The remaining modulated neurons (n = 69 of 142 neurons) were designated as "Opto-modulated". We cannot exclude that some of the putative S1-projecting ClaC neurons are not S1-projecting because the synchronous activation of excitatory neurons may rapidly excite a postsynaptic neuron that itself does not express ChR2. However, the criteria used were similar to standards in the field (Kvitsiani et al., 2013). Furthermore, although some studies using anatomical tracers (Smith and Alloway, 2010) or population-based multielectrode recording methods (Orman, 2015) suggest that there exist some excitatory connections among claustrum neurons, electrophysiological evidence from paired recordings indicate that the monosynaptic connectivity among excitatory neurons in the claustrum is low (2%, n = 2 of 86 tested pairs, Kim et al., 2016). A more extended discussion of these issues can be found in Jackson et al., 2020. It is also possible that some S1-projecting ClaC neurons may be included in our non-optotagged sample although retro-AAV is highly efficient at transducing ClaC neurons (Marriott et al., 2021). Thus, while we cannot rule out the possibility that our optotagging strategy misidentified a subset of S1-projecting ClaC neurons, it allowed us to reliably establish that our electrodes were within the claustrum.

Immunohistochemistry—Following recordings and lesions, mice were transcardially perfused with 0.01 M phosphate buffered saline (PBS) followed by 4% paraformaldehyde (PFA) solution, and brains were post-fixed for 3 h at room temperature in 4% PFA. Then, 60 μm sections were cut on a vibratome (VT-1000S, Leica) and processed for immunohistochemistry (1:1000, Rabbit anti-DsRed polyclonal antibody, Living Colors, Clontech Laboratories, RRID: AB_10013483 and Alexa Fluor Donkey anti-Rabbit IgG (H+L) Highly Cross-Adsorbed Secondary Antibody, ThermoFisher (Invitrogen), A-21207, RRID: AB_141637; 1:1000, Chicken anti-GFP, GFP-1020, Aves, RRID:AB_10000240 and Alexa Fluor 488 AffiniPure Donkey anti-Chicken IgY (IgG) (H+L) antibody, Jackson ImmunoResearch Laboratories Inc, 703–545-155, RRID:AB_2340375; 1:200 Rabbit anti-parvalbumin, PV27, Swant, RRID: AB_2631173 and Alexa647-conjugated Donkey anti-Rabbit, Jackson ImmunoResearch Laboratories Inc, 711–606-152, RRID:AB_2340625). Specifically, sections were incubated in blocking solution (3% Normal Donkey Serum, 0.3% TritonX-100 in PBS) for 2 hours on a rocker, followed by overnight incubation at 4°C with the primary antibodies (diluted in blocking solution). The following day, sections were rinsed 3 times for 10 min in PBS and incubated for 2 hours at room temperature with secondary antibodies diluted in blocking solution. Sections were then rinsed 3 times for 10 min before mounting. Animals used in the chemogenetic experiments were processed similarly (1:1000, Rabbit anti-DsRed polyclonal antibody, Living Colors, Clontech Laboratories, RRID: AB_10013483 and Alexa Fluor 594 Donkey anti-Rabbit IgG

(H+L) Highly Cross-Adsorbed Secondary Antibody ThermoFisher (Invitrogen)). Animals used for visualizing corticoclaustral projections from ALM (Figure S4D–J) were also processed similarly (1:2000, Chicken anti-GFP, GFP-1020, Aves, RRID:AB_10000240, and 1:1000 AlexaFluor 488-conjugated Donkey anti-Chicken, Jackson ImmunoResearch Labs, 703–545-155, RRID: AB_2340375; 1:1000 Mouse anti-parvalbumin, Sigma-Aldrich, P3088, RRID: AB_477329, and 1:1000 DyLight 405-AffiniPure Donkey anti-Mouse IgG (H+L), Jackson ImmunoResearch Labs, 715–475-150, RRID: AB_2340839).

Sections were then mounted using Aqua Poly/Mount mounting medium (Polysciences, Inc) and visualized on a confocal microscope (LSM 510 or 800, Zeiss) using 10x (0.3 NA), 20x (0.8 NA) or 40x (1.3 NA) objectives or on an epifluorescence microscope (BZ-X 710, Keyence) using a 4x objective. Images were processed using ImageJ (Schneider et al., 2012).

Figure 1E and F are maximum projections of confocal image stacks. The bright tetrode tracks prevent visualization of the tdTomato-positive Cre-expressing neurons in Figure 1E.

DREADD inactivation experiment—The experimenter was blinded to the identity of each animal (n = 6 hM4Di-mCherry mice, 2 males and 4 females; n = 5 mCherry mice, 1 male and 4 females). Mice were trained similarly to mice used for *in vivo* electrophysiological recordings until they reached 65% or higher correct trials for three consecutive days. Once trained, animals were injected intraperitoneally with either the DREADD receptor agonist Agonist 21 dihydrochloride (Tocris 6422, 3 mg/kg in 0.9% NaCl) or vehicle (0.9% NaCl, same volume as previous agonist session) 30 min prior to the start of the behavioral session. Injections of agonist and vehicle were alternated on consecutive days for 8 days, resulting in 4 “treated” and 4 “saline” sessions per animal but for one control animal expressing mCherry who completed only 3 “saline” sessions.

QUANTIFICATION AND STATISTICAL ANALYSIS

Statistical tests and sample size—The details of all statistical tests performed are described in the main text, figure legends and supplementary figure legends. Sample sizes are similar to other studies in the field.

Identification of responsive neurons—To determine whether individual neurons were modulated during distinct trial types (Figure 2C–F, 3A–D), we compared the distributions of spike counts one second preceding stimulus onset to the spike counts during the one second following stimulus onset (Mann-Whitney U tests).

Linear Discriminant Analysis—To quantify the correlations between various task variables and variations in neural activity, we performed Linear Discriminant Analyses (LDA) on recordings from each behavioral session. Specifically, we first built a trial_x_neuron matrix in which the value in each bin was the number of spikes in the one second following stimulus onset. We randomly drew 80% of the trials in each behavioral session to train the LDA and set the remaining 20% aside for testing. The LDA was trained to identify the linear combination of simultaneously recorded neurons whose spike counts best predicted the class of a trial. We applied the trained LDA to the remaining 20% of trials,

and classification accuracy was determined. This process was repeated 50 times for each behavioral session. The final score for a session was taken as the average accuracy over the 50 iterations. This procedure was performed to classify trials based on stimulus type (Tactile stimulus vs Visual stimulus), block type (Respond-to-Touch block vs Respond-to-Light block) and response type (Lick vs No Lick).

Ideal observer analysis—We used a receiver operating characteristic analysis to quantify how well individual neurons discriminated between two types of trials. Stimulus-aligned spike counts from single trials were binned in 25 ms bins ranging from −1 s to 3 s following the sensory stimulus presentation. For each bin, we grouped spike counts based on their trial type (for example, lick trial vs no_lick trial) and quantified the separation between these two distributions using the Area Under the ROC Curve score (Python 3 scikit_learn version 0.19.1 function: roc_auc_score). The ROC curve was built by plotting the true-positive rate against the false-positive rate upon varying the cut-off between the two distributions along all possible values. We computed a 95% confidence interval for each bin by performing this analysis on resampled data (with replacement) and bootstrapping 1000 times. A unit was considered to significantly distinguish between the two trial types if the lower bound of the 95% confidence interval was greater than 0.5 for 3 consecutive 25 ms bins or if the upper bound of the 95% confidence interval was smaller than 0.5 for 3 consecutive 25 ms bins. The first of these bins was taken as the onset time.

Activity onset determination—To determine the onset of spontaneous lick-related activity (Figure S5B,C), we first identified significantly modulated claustrum neurons by comparing the distributions of spike counts from −2 to −1 seconds preceding spout contact to the spike counts surrounding the spout contact (−0.5 s to +0.5 s, Mann-Whitney U tests). For each significantly modulated neuron, we identified the onset of modulation as the time at which the mean lick-aligned activity became greater or smaller than 3 standard deviations from the baseline mean computed from −2 to −1 seconds preceding the lick for 100 consecutive milliseconds.

Decoder—The decoder we used was developed in Mayrhofer et al., 2019 and based on ideas presented in Jazayeri and Movshon, 2006 and Ma et al., 2006. The goal of the decoder is to predict whether the mouse licked the ipsilateral or contralateral spout in response to a sensory stimulus using the baseline preferences of individual neurons for lick direction during spontaneous licks. We used the mean response to spontaneous licks occurring during the intertrial periods as the contralateral lick tuning and ipsilateral lick tuning. For lick bouts, we included the first lick but excluded all subsequent licks from the analysis. We restricted our analyses to behavioral sessions with recordings from at least 6 responsive neurons. A neuron was considered responsive if its mean activity in the 500 ms surrounding the lick (−250 ms to + 250 ms) was significantly different from the activity during a 500 ms baseline period, −2 to −1.5 s prior to a lick (two-tailed Kolmogorov-Smirnov test) and if at least 30 spontaneous licks to each lick port were available from the session to compute the mean response. To generate the predictions, we first built a population matrix with each row representing a trial and each column the z-scored response of each neuron (mean activity in the 500 ms surrounding the detection-associated lick, from −250 ms to +250

ms). This matrix was multiplied by the log of the tuning curves (i.e., the mean responses to contralateral licks and ipsilateral licks), resulting in a log-likelihood for contralateral lick and ipsilateral lick for each trial. Before matrix multiplication, the mean log-tuning curves from a session were subtracted from each neuron's log-tuning curves to correct for the session's response bias. The final prediction of the decoder consisted of the lick direction with the largest log-likelihood and was compared to the true lick direction to compute the decoding accuracy.

Hierarchical clustering—We used hierarchical clustering to organize neurons based on their response profile. For each neuron, we constructed a vector representing the mean stimulus-aligned activity during touch-associated lick trials followed by the mean stimulus-aligned activity during vision-associated lick trials (25 ms bins, −1 to 3 s following the sensory stimulus presentation for each trial type; final vector length = 320 bins). We used this vector as input to compute the pairwise Pearson correlation between all pairs of neurons and applied hierarchical clustering (average method) on the resulting neuron_x_neuron matrix (containing the correlation coefficients). The groups displayed in Figure S7 were defined by using a cutoff of 5.0 on the dendrogram.

Lick Direction Preference Index and Upcoming Lick Direction Index—To determine the preference of each neuron for spontaneous contralateral versus ipsilateral licks, we computed the Lick Direction Preference Index, (C-I)/(C+I), where C and I are the mean firing rates of a neuron during the 200 ms, −100 ms to 100 ms, surrounding spontaneous, non-bout, lick port contacts occurring during the intertrial intervals. Non-bout licks included individual licks separated by at least 500 ms from any preceding or following lick as well as the first lick of lick bouts defined as a series of licks separated by < 500 ms between two licks. The Upcoming Lick Direction Index was calculated similarly to the Lick Direction Preference Index, using the mean firing rate during the 1 s preceding the delivery of the sensory stimulus during Contralateral-lick blocks versus during Ipsilateral-lick blocks. Trials in which the mouse spontaneously licked during the 1 s preceding stimulus presentation were omitted in Figure 6B and in the calculations of the Upcoming Lick Direction Index.

Cross-correlograms—The analysis of synchronous activity included only neurons that were recorded with tetrodes in the claustrum or S1. To compute the cross-correlogram for each pair of simultaneously recorded neurons, we followed the procedure described in Kohn and Smith, 2005. For each trial, we converted the time stamps of action potentials occurring during the one second preceding presentation of the sensory stimulus into a binary vector of 1 ms resolution (1000 bins, either zero, or one if a spike occurred during that bin interval). We used the function 'correlate' from the scipy package (Python 3) to compute the correlation between the two binary vectors at each time lag to generate the cross-correlogram. The resulting vector was normalized (binwise) by the triangular function (1-|lag| in seconds), to correct for the degree of overlap between the two binary vectors for each time lag, and by the geometric mean of the firing rates of the two spike trains (Hz). The trialwise correlations were summed and normalized by the number of trials for each pair of neurons. Finally, the resulting cross-correlograms (CCGs) were corrected by subtracting the

segment-shifted cross-correlogram (neuronA prestimulus segment t vs neuronB prestimulus segment t+1). The final cross-correlogram was convolved with the following vector [0.05, 0.25, 0.4, 0.25, 0.05] to smooth the shift-corrected cross-correlograms. Significantly correlated pairs were identified as those with a peak greater than 5 SD above the mean taken at [−500 ms to −400 ms]U[400 ms to 500 ms]. Only pairs for which each neuron was recorded on a different tetrode and for which both neurons had at least 30 trials with at least one spike in each were included in our analysis. Eight mice contributed the 75 pairs of significantly correlated claustrum neurons using the 1 s preceding stimulus onset, and five mice contributed the subset of 27 significantly correlated pairs of claustrum neurons for which both neurons exhibited strong lick direction preferences. The location of the cortical S1 recordings was unknown with respect to cortical layers. The width of each crosscorrelogram was taken as the interval between the time at which three consecutive 1 millisecond bins rose 3 standard deviations or more above the baseline mean prior to the CCG peak and the time at which three consecutive millisecond bins fell below 3 standard deviations above the baseline mean following the CCG peak.

Supplementary Material

Refer to Web version on PubMed Central for supplementary material.

ACKNOWLEDGMENTS

The authors thank J.Y. Cohen and members of the Brown and O'Connor labs for thoughtful input. This work was supported by the National Institutes of Neurological Diseases (R01NS085121, R01NS089652, 1R01NS104834-01, P30NS050274) and a Johns Hopkins Discovery Award. M.C. was supported by a Boehringer-Ingelheim Fonds Fellowship.

REFERENCES

Alexander GE, and Crutcher MD (1990). Neural representations of the target (goal) of visually guided arm movements in three motor areas of the monkey. J Neurophysiol 64, 164–178. [PubMed: 2388063]

Alloway KD, Smith JB, Beauchemin KJ, and Olson ML (2009). Bilateral projections from rat MI whisker cortex to the neostriatum, thalamus, and claustrum: forebrain circuits for modulating whisking behavior. J Comp Neurol 515, 548–564. [PubMed: 19479997]

Atlan G, Matosevich N, Peretz-Rivlin N, Yvgi I, Chen ES, Kleinman T, Bleistein N, Scheinbach E, Groysman M, Nir Y, et al. (2021). Claustral projections to anterior cingulate cortex modulate engagement with the external world. bioRxiv 10.1101/2021.06.17.448649.

Atlan G, Terem A, Peretz-Rivlin N, Groysman M, and Citri A (2017). Mapping synaptic cortico-claustral connectivity in the mouse. J Comp Neurol 525, 1381–1402. [PubMed: 26973027]

Atlan G, Terem A, Peretz-Rivlin N, Sehrawat K, Gonzales BJ, Pozner G, Tasaka GI, Goll Y, Refaeli R, Zviran O, et al. (2018). The claustrum supports resilience to distraction. Curr Biol 28, 2752–2762 e2757. [PubMed: 30122531]

Boyden ES, Zhang F, Bamberg E, Nagel G, and Deisseroth K (2005). Millisecond-timescale, genetically targeted optical control of neural activity. Nat Neurosci 8, 1263–1268. [PubMed: 16116447]

Brooks JX, and Cullen KE (2019). Predictive sensing: The role of motor signals in sensory processing. Biol Psychiatry Cogn Neurosci Neuroimaging 4, 842–850. [PubMed: 31401034]

Brown SP, Mathur BN, Olsen SR, Luppi PH, Bickford ME, and Citri A (2017). New breakthroughs in understanding the role of functional interactions between the neocortex and the claustrum. J Neurosci 37, 10877–10881. [PubMed: 29118217]

Chabrol FP, Blot A, and Mrsic-Flogel TD (2019). Cerebellar contribution to preparatory activity in motor neocortex. Neuron 103, 506–519 e504. [PubMed: 31201123]

Chen TW, Li N, Daie K, and Svoboda K (2017). A map of anticipatory activity in mouse motor cortex. Neuron 94, 866–879 e864. [PubMed: 28521137]

Chia Z, Augustine GJ, and Silberberg G (2020). Synaptic connectivity between the cortex and claustrum is organized into functional modules. Curr Biol 30, 2777–2790 e2774. [PubMed: 32531275]

Clarey JC, and Irvine DRF (1986). Auditory response properties of neurons in the claustrum and putamen of the cat. Experimental Brain Research 61, 432–437. [PubMed: 3948949]

Clascá F, Avendaño C, Román-Guindo A, Llamas A, and Reinoso-Suárez F (1992). Innervation from the claustrum of the frontal association and motor areas - axonal-transport studies in the cat. J Comp Neurol 326, 402–422. [PubMed: 1281846]

Cohen JY, Haesler S, Vong L, Lowell BB, and Uchida N (2012). Neuron-type-specific signals for reward and punishment in the ventral tegmental area. Nature 482, 85–88. [PubMed: 22258508]

Cortimiglia R, Crescimanno G, Salerno MT, and Amato G (1991). The role of the claustrum in the bilateral control of frontal oculomotor neurons in the cat. Exp Brain Res 84, 471–477. [PubMed: 1864320]

Cortimiglia R, Crescimanno G, Salerno MT, Amato G, and Infantellina F (1987). Electrophysiological relationship between claustrum and contralateral area 4 and 6 pyramidal tract neurons. Neurosci Lett 74, 193–198. [PubMed: 3574758]

Cousineau D, and Chartier S (2010). Outliers detection and treatment: A review. International Journal of Psychological Research 3, 58–67.

Crescimanno G, Salerno MT, Cortimiglia R, and Amato G (1989). Claustral influence on ipsi- and contralateral motor cortical areas, in the cat. Brain Research Bulletin 22, 839–843. [PubMed: 2765944]

Crescimanno G, Salerno MT, Cortimiglia R, and Amato G (1990). Effect of claustrum stimulation on neurons of the contralateral medial oculomotor area, in the cat. Neurosci Lett 114, 289–294. [PubMed: 2402337]

Crescimanno G, Salerno MT, Cortimiglia R, Amato G, and Infantellina F (1984). Functional relationship between claustrum and pyramidal tract neurons, in the cat. Neurosci Lett 44, 125–129. [PubMed: 6709227]

Crick FC, and Koch C (2005). What is the function of the claustrum? Philosophical Transactions of the Royal Society B-Biological Sciences 360, 1271–1279.

Druga R, Chen S, and Bentivoglio M (1993). Parvalbumin and calbindin in the rat claustrum: an immunocytochemical study combined with retrograde tracing frontoparietal cortex. J Chem Neuroanat 6, 399–406. [PubMed: 8142075]

Ebbesen CL, and Brecht M (2017). Motor cortex - to act or not to act? Nat Rev Neurosci 18, 694–705. [PubMed: 29042690]

Economo MN, Viswanathan S, Tasic B, Bas E, Winnubst J, Menon V, Graybuck LT, Nguyen TN, Smith KA, Yao Z, et al. (2018). Distinct descending motor cortex pathways and their roles in movement. Nature 563, 79–84. [PubMed: 30382200]

Esmaeili V, Tamura K, Muscinelli SP, Modirshanechi A, Boscaglia M, Lee AB, Oryshchuk A, Foustoukos G, Liu Y, Crochet S, et al. (2021). Rapid suppression and sustained activation of distinct cortical regions for a delayed sensory-triggered motor response. Neuron 109, 2183–2201 e2189. [PubMed: 34077741]

Goard MJ, Pho GN, Woodson J, and Sur M (2016). Distinct roles of visual, parietal, and frontal motor cortices in memory-guided sensorimotor decisions. Elife 5, e13764. [PubMed: 27490481]

Goll Y, Atlan G, and Citri A (2015). Attention: The claustrum. Trends Neurosci 38, 486–495. [PubMed: 26116988]

Guo ZV, Inagaki HK, Daie K, Druckmann S, Gerfen CR, and Svoboda K (2017). Maintenance of persistent activity in a frontal thalamocortical loop. Nature 545, 181–186. [PubMed: 28467817]

Guo ZV, Li N, Huber D, Ophir E, Gutnisky D, Ting JT, Feng G, and Svoboda K (2014). Flow of cortical activity underlying a tactile decision in mice. Neuron 81, 179–194. [PubMed: 24361077]

Hinova-Palova DV, Edelstein LR, Paloff AM, Hristov S, Papantchev VG, and Ovtscharoff WA (2007). Parvalbumin in the cat claustrum: Ultrastructure, distribution and functional implications. Acta Histochemica 109, 61–77. [PubMed: 17126385]

Hu F, Kamigaki T, Zhang Z, Zhang S, Dan U, and Dan Y (2019). Prefrontal corticotectal neurons enhance visual processing through the superior colliculus and pulvinar thalamus. Neuron 104, 1141–1152 e1144. [PubMed: 31668485]

Huber D, Gutnisky DA, Peron S, O'Connor DH, Wiegert JS, Tian L, Oertner TG, Looger LL, and Svoboda K (2012). Multiple dynamic representations in the motor cortex during sensorimotor learning. Nature 484, 473–478. [PubMed: 22538608]

Inagaki HK, Fontolan L, Romani S, and Svoboda K (2019). Discrete attractor dynamics underlies persistent activity in the frontal cortex. Nature 566, 212–217. [PubMed: 30728503]

Inagaki HK, Inagaki M, Romani S, and Svoboda K (2018). Low-dimensional and monotonic preparatory activity in mouse anterior lateral motor cortex. J Neurosci 38, 4163–4185. [PubMed: 29593054]

Jackson J, Karnani MM, Zemelman BV, Burdakov D, and Lee AK (2018). Inhibitory control of prefrontal cortex by the claustrum. Neuron 99, 1029–1039 e1024. [PubMed: 30122374]

Jackson J, Smith JB, and Lee AK (2020). The anatomy and physiology of claustrum-cortex interactions. Annu Rev Neurosci 43, 231–247. [PubMed: 32084328]

Jankowski MM, and O'Mara SM (2015). Dynamics of place, boundary and object encoding in rat anterior claustrum. Front Behav Neurosci 9, 250. [PubMed: 26557060]

Jazayeri M, and Movshon JA (2006). Optimal representation of sensory information by neural populations. Nat Neurosci 9, 690–696. [PubMed: 16617339]

Kamigaki T, and Dan Y (2017). Delay activity of specific prefrontal interneuron subtypes modulates memory-guided behavior. Nat Neurosci 20, 854–863. [PubMed: 28436982]

Kim J, Matney CJ, Roth RH, and Brown SP (2016). Synaptic organization of the neuronal circuits of the claustrum. J Neurosci 36, 773–784. [PubMed: 26791208]

Kohn A, and Smith MA (2005). Stimulus dependence of neuronal correlation in primary visual cortex of the macaque. J Neurosci 25, 3661–3673. [PubMed: 15814797]

Komiyama T, Sato TR, O'Connor DH, Zhang YX, Huber D, Hooks BM, Gabitto M, and Svoboda K (2010). Learning-related fine-scale specificity imaged in motor cortex circuits of behaving mice. Nature 464, 1182–1186. [PubMed: 20376005]

Krashes MJ, Koda S, Ye C, Rogan SC, Adams AC, Cusher DS, Maratos-Flier E, Roth BL, and Lowell BB (2011). Rapid, reversible activation of AgRP neurons drives feeding behavior in mice. J Clin Invest 121, 1424–1428. [PubMed: 21364278]

Kvitsiani D, Ranade S, Hangya B, Taniguchi H, Huang JZ, and Kepecs A (2013). Distinct behavioural and network correlates of two interneuron types in prefrontal cortex. Nature 498, 363–366. [PubMed: 23708967]

Le Merre P, Esmaeili V, Charriere E, Galan K, Salin PA, Petersen CCH, and Crochet S (2018). Reward-based learning drives rapid sensory signals in medial prefrontal cortex and dorsal hippocampus necessary for goal-directed behavior. Neuron 97, 83–91 e85. [PubMed: 29249287]

LeVay S, and Sherk H (1981a). The visual claustrum of the cat. I. Structure and connections. J Neurosci 1, 956–980. [PubMed: 6169810]

LeVay S, and Sherk H (1981b). The visual claustrum of the cat. II. The visual field map. J Neurosci 1, 981–992. [PubMed: 6169811]

Lévesque M, and Parent A (1998). Axonal arborization of corticostriatal and corticothalamic fibers arising from prelimbic cortex in the rat. Cerebral Cortex 8, 602–613. [PubMed: 9823481]

Li B, Nguyen TP, Ma C, and Dan Y (2020). Inhibition of impulsive action by projection-defined prefrontal pyramidal neurons. Proc Natl Acad Sci U S A 117, 17278–17287. [PubMed: 32631999]

Li N, Chen TW, Guo ZV, Gerfen CR, and Svoboda K (2015). A motor cortex circuit for motor planning and movement. Nature 519, 51–56. [PubMed: 25731172]

Li N, Daie K, Svoboda K, and Druckmann S (2016). Robust neuronal dynamics in premotor cortex during motor planning. Nature 532, 459–464. [PubMed: 27074502]

Liu J, Wu R, Johnson B, Vu J, Bass C, and Li JX (2019). The claustrum-prefrontal cortex pathway regulates impulsive-like behavior. J Neurosci 39, 10071–10080. [PubMed: 31704786]

Ma WJ, Beck JM, Latham PE, and Pouget A (2006). Bayesian inference with probabilistic population codes. Nat Neurosci 9, 1432–1438. [PubMed: 17057707]

Macchi G, Bentivoglio M, Minciacchi D, and Molinari M (1981). The organization of the claustroneocortical projections in the cat studied by means of the HRP retrograde axonal transport. J Comp Neurol 195, 681–695. [PubMed: 6161950]

Madisen L, Garner AR, Shimaoka D, Chuong AS, Klapoetke NC, Li L, van der Bourg A, Niino Y, Egolf L, Monetti C, et al. (2015). Transgenic mice for intersectional targeting of neural sensors and effectors with high specificity and performance. Neuron 85, 942–958. [PubMed: 25741722]

Madisen L, Zwingman TA, Sunkin SM, Oh SW, Zariwala HA, Gu H, Ng LL, Palmiter RD, Hawrylycz MJ, Jones AR, et al. (2010). A robust and high-throughput Cre reporting and characterization system for the whole mouse brain. Nat Neurosci 13, 133–140. [PubMed: 20023653]

Manita S, Suzuki T, Homma C, Matsumoto T, Odagawa M, Yamada K, Ota K, Matsubara C, Inutsuka A, Sato M, et al. (2015). A top-down cortical circuit for accurate sensory perception. Neuron 86, 1304–1316. [PubMed: 26004915]

Marriott BA, Do AD, Zahacy R, and Jackson J (2021). Topographic gradients define the projection patterns of the claustrum core and shell in mice. J Comp Neurol 529, 1607–1627. [PubMed: 32975316]

Massion J (1992). Movement, posture and equilibrium: interaction and coordination. Prog Neurobiol 38, 35–56. [PubMed: 1736324]

Mathur BN, Caprioli RM, and Deutch AY (2009). Proteomic analysis illuminates a novel structural definition of the claustrum and insula. Cerebral Cortex 19, 2372–2379. [PubMed: 19168664]

Mayrhofer JM, El-Boustani S, Foustoukos G, Auffret M, Tamura K, and Petersen CCH (2019). Distinct contributions of whisker sensory cortex and tongue-jaw motor cortex in a goal-directed sensorimotor transformation. Neuron 103, 1034–1043 e1035. [PubMed: 31402199]

Minamisawa G, Kwon SE, Chevée M, Brown SP, and O'Connor DH (2018). A non-canonical feedback circuit for rapid interactions between somatosensory cortices. Cell Rep 23, 2718–2731. [PubMed: 29847801]

Murakami M, Vicente MI, Costa GM, and Mainen ZF (2014). Neural antecedents of self-initiated actions in secondary motor cortex. Nat Neurosci 17, 1574–1582. [PubMed: 25262496]

Musall S, Kaufman MT, Juavinett AL, Gluf S, and Churchland AK (2019). Single-trial neural dynamics are dominated by richly varied movements. Nat Neurosci 22, 1677–1686. [PubMed: 31551604]

Narikiyo K, Mizuguchi R, Ajima A, Shiozaki M, Hamanaka H, Johansen JP, Mori K, and Yoshihara Y (2020). The claustrum coordinates cortical slow-wave activity. Nat Neurosci 23, 741–753. [PubMed: 32393895]

Nienborg H, Cohen MR, and Cumming BG (2012). Decision-related activity in sensory neurons: correlations among neurons and with behavior. Annu Rev Neurosci 35, 463–483. [PubMed: 22483043]

Norimoto H, Fenk LA, Li HH, Tosches MA, Gallego-Flores T, Hain D, Reiter S, Kobayashi R, Macias A, Arends A, et al. (2020). A claustrum in reptiles and its role in slow-wave sleep. Nature 578, 413–418. [PubMed: 32051589]

Olson CR, and Graybiel AM (1980). Sensory maps in the claustrum of the cat. Nature 288, 479–481. [PubMed: 7442793]

Orman R (2015). Claustrum: a case for directional, excitatory, intrinsic connectivity in the rat. J Physiol Sci 65, 533–544. [PubMed: 26329935]

Parent M, and Parent A (2006). Single-axon tracing study of corticostriatal projections arising from primary motor cortex in primates. J Comp Neurol 496, 202–213. [PubMed: 16538675]

Petreanu L, Gutnisky DA, Huber D, Xu NL, O'Connor DH, Tian L, Looger L, and Svoboda K (2012). Activity in motor-sensory projections reveals distributed coding in somatosensation. Nature 489, 299–303. [PubMed: 22922646]

Ptito M, and Lassonde MC (1981). Effects of claustral stimulation on the properties of visual cortex neurons in the cat. Exp Neurol 73, 315–320. [PubMed: 7250286]

Rahman FE, and Baizer JS (2007). Neurochemically defined cell types in the claustrum of the cat. Brain Research 1159, 94–111. [PubMed: 17582386]

Remedios R, Logothetis NK, and Kayser C (2010). Unimodal responses prevail within the multisensory claustrum. J Neurosci 30, 12902–12907. [PubMed: 20881109]

Remedios R, Logothetis NK, and Kayser C (2014). A role of the claustrum in auditory scene analysis by reflecting sensory change. Front Syst Neurosci 8, 44. [PubMed: 24772069]

Renouard L, Billwiller F, Ogawa K, Clement O, Camargo N, Abdelkarim M, Gay N, Scote-Blachon C, Toure R, Libourel PA, et al. (2015). The supramammillary nucleus and the claustrum activate the cortex during REM sleep. Sci Adv 1, e1400177. [PubMed: 26601158]

Riehle A, and Requin J (1989). Monkey primary motor and premotor cortex: single-cell activity related to prior information about direction and extent of an intended movement. J Neurophysiol 61, 534–549. [PubMed: 2709098]

Salerno MT, Cortimiglia R, Crescimanno G, and Amato G (1989). Effect of claustrum activation on the spontaneous unitary activity of frontal eye field neurons in the cat. Neurosci Lett 98, 299–304. [PubMed: 2725949]

Salerno MT, Cortimiglia R, Crescimanno G, Amato G, and Infantellina F (1984). Effects of claustrum stimulation on spontaneous bioelectrical activity of motor cortex neurons in the cat. Exp Neurol 86, 227–239. [PubMed: 6489496]

Salkoff DB, Zagha E, McCarthy E, and McCormick DA (2020). Movement and performance explain widespread cortical activity in a visual detection task. Cereb Cortex 30, 421–437. [PubMed: 31711133]

Schneider CA, Rasband WS, and Eliceiri KW (2012). NIH Image to ImageJ: 25 years of image analysis. Nat Methods 9, 671–675. [PubMed: 22930834]

Schneider DM, Sundararajan J, and Mooney R (2018). A cortical filter that learns to suppress the acoustic consequences of movement. Nature 561, 391–395. [PubMed: 30209396]

Sherk H, and LeVay S (1981). The visual claustrum of the cat. III. Receptive field properties. J Neurosci 1, 993–1002. [PubMed: 6169812]

Shima K, Hoshi E, and Tanji J (1996). Neuronal activity in the claustrum of the monkey during performance of multiple movements. Journal of Neurophysiology 76, 2115–2119. [PubMed: 8890324]

Sippy T, Lapray D, Crochet S, and Petersen CC (2015). Cell-type-specific sensorimotor processing in striatal projection neurons during goal-directed behavior. Neuron 88, 298–305. [PubMed: 26439527]

Smith JB, and Alloway KD (2010). Functional specificity of claustrum connections in the rat: interhemispheric communication between specific parts of motor cortex. J Neurosci 30, 16832–16844. [PubMed: 21159954]

Smith JB, and Alloway KD (2014). Interhemispheric claustral circuits coordinate sensory and motor cortical areas that regulate exploratory behaviors. Front Syst Neurosci 8, 93. [PubMed: 24904315]

Smith JB, Radhakrishnan H, and Alloway KD (2012). Rat claustrum coordinates but does not integrate somatosensory and motor cortical information. J Neurosci 32, 8583–8588. [PubMed: 22723699]

Smith JB, Watson GDR, Liang Z, Liu Y, Zhang N, and Alloway KD (2019). A role for the claustrum in salience processing? Front Neuroanat 13, 64. [PubMed: 31275119]

Smythies J, Edelstein L, and Ramachandran V (2012). Hypotheses relating to the function of the claustrum. Front Integr Neurosci 6, 53. [PubMed: 22876222]

Smythies J, Edelstein L, and Ramachandran V (2014). Hypotheses relating to the function of the claustrum II: does the claustrum use frequency codes? Front Integr Neurosci 8, 7. [PubMed: 24523681]

Squire RF, Noudoost B, Schafer RJ, and Moore T (2013). Prefrontal contributions to visual selective attention. Annu Rev Neurosci 36, 451–466. [PubMed: 23841841]

Steinmetz NA, and Moore T (2010). Changes in the response rate and response variability of area V4 neurons during the preparation of saccadic eye movements. J Neurophysiol 103, 1171–1178. [PubMed: 20018834]

Stringer C, Pachitariu M, Steinmetz N, Reddy CB, Carandini M, and Harris KD (2019). Spontaneous behaviors drive multidimensional, brainwide activity. Science 364, 255. [PubMed: 31000656]

Svoboda K, and Li N (2018). Neural mechanisms of movement planning: motor cortex and beyond. Curr Opin Neurobiol 49, 33–41. [PubMed: 29172091]

Tanné-Gariépy J, Boussaoud D, and Rouiller EM (2002). Projections of the claustrum to the primary motor, premotor, and prefrontal cortices in the macaque monkey. J Comp Neurol 454, 140–157. [PubMed: 12412139]

Terem A, Gonzales BJ, Peretz-Rivlin N, Ashwal-Fluss R, Bleistein N, Reus-García MM, Mukherjee D, Groysman M, and Citri A (2020). Claustral neurons projecting to frontal cortex mediate contextual association of reward. Curr Biol 30, 3522–3532 e3526. [PubMed: 32707061]

Tervo DG, Hwang BY, Viswanathan S, Gaj T, Lavzin M, Ritola KD, Lindo S, Michael S, Kuleshova E, Ojala D, et al. (2016). A designer AAV variant permits efficient retrograde access to projection neurons. Neuron 92, 372–382. [PubMed: 27720486]

Torgerson CM, Irimia A, Goh SY, and Van Horn JD (2015). The DTI connectivity of the human claustrum. Hum Brain Mapp 36, 827–838. [PubMed: 25339630]

Tsumoto T, and Suda K (1982). Effects of stimulation of the dorsocaudal claustrum on activities of striate cortex neurons in the cat. Brain Res 240, 345–349. [PubMed: 7104694]

Vidyasagar TR, and Levichkina E (2019). An integrated neuronal model of claustral function in timing the synchrony between cortical areas. Front Neural Circuits 13, 3. [PubMed: 30804759]

Wang Q, Ng L, Harris JA, Feng D, Li Y, Royall JJ, Oh SW, Bernard A, Sunkin SM, Koch C, et al. (2017). Organization of the connections between claustrum and cortex in the mouse. J Comp Neurol 525, 1317–1346. [PubMed: 27223051]

White MG, Cody PA, Bubser M, Wang HD, Deutch AY, and Mathur BN (2017). Cortical hierarchy governs rat claustrocortical circuit organization. J Comp Neurol 525, 1347–1362. [PubMed: 26801010]

White MG, and Mathur BN (2018a). Claustrum circuit components for top-down input processing and cortical broadcast. Brain Struct Funct 223, 3945–3958. [PubMed: 30109490]

White MG, and Mathur BN (2018b). Frontal cortical control of posterior sensory and association cortices through the claustrum. Brain Struct Funct 223, 2999–3006. [PubMed: 29623428]

White MG, Mu C, Qadir H, Madden MB, Zeng H, and Mathur BN (2020). The mouse claustrum is required for optimal behavioral performance under high cognitive demand. Biol Psychiatry 88, 719–726. [PubMed: 32456782]

White MG, Panicker M, Mu C, Carter AM, Roberts BM, Dharmasri PA, and Mathur BN (2018). Anterior cingulate cortex input to the claustrum is required for top-down action control. Cell Rep 22, 84–95. [PubMed: 29298436]

Wimmer RD, Schmitt LI, Davidson TJ, Nakajima M, Deisseroth K, and Halassa MM (2015). Thalamic control of sensory selection in divided attention. Nature 526, 705–709. [PubMed: 26503050]

Wu Z, Litwin-Kumar A, Shamash P, Taylor A, Axel R, and Shadlen MN (2020). Context-dependent decision making in a premotor circuit. Neuron 106, 316–328 e316. [PubMed: 32105611]

Zagha E, Casale AE, Sachdev RN, McGinley MJ, and McCormick DA (2013). Motor cortex feedback influences sensory processing by modulating network state. Neuron 79, 567–578. [PubMed: 23850595]

Zagha E, Ge X, and McCormick DA (2015). Competing neural ensembles in motor cortex gate goal-directed motor output. Neuron 88, 565–577. [PubMed: 26593093]

Zingg B, Dong HW, Tao HW, and Zhang LI (2018). Input-output organization of the mouse claustrum. J Comp Neurol 526, 2428–2443. [PubMed: 30252130]

Zingg B, Hintiryan H, Gou L, Song MY, Bay M, Bienkowski MS, Foster NN, Yamashita S, Bowman I, Toga AW, et al. (2014). Neural networks of the mouse neocortex. Cell 156, 1096–1111. [PubMed: 24581503]

HIGHLIGHTS

- Anterior claustrum neurons exhibit motor responses
- Claustrum neurons, including S1-projecting neurons, encode lick direction
- Neuron pairs with synchronous firing during intertrial intervals are similarly tuned
- Chemogenetic inhibition of claustrocortical neurons decreases false alarms

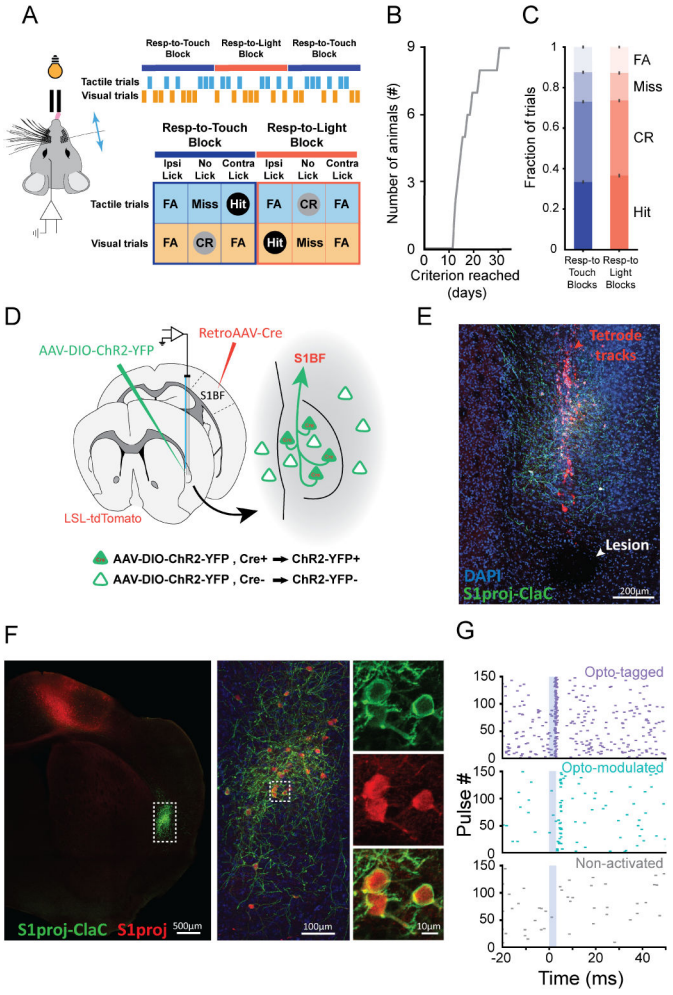

Figure 1. Behavioral task and recording strategy

(A) Behavioral set-up. Response types for mice trained on Tactile stim→lick contralateral, Visual stim→lick ipsilateral are shown (CR: Correct Rejection, FA: False Alarm).

(B) Time to learn task (n = 9 mice; 6 tactile stim→lick contralateral, 3 tactile stim→lick ipsilateral).

(C) Trial outcomes across all sessions (error bars: SEM, n = 9 mice, 73 sessions; Hits: 0.33 ± 0.0085; CRs: 0.37 ± 0.0076; Misses: 0.15 ± 0.0080; FAs: 0.12 ± 0.0064).

(D) Viral expression and recording strategy.

(E) Tetrode tracks (red) traversing the claustrum, ChR2-YFP-expressing putative S1-projecting claustrocortical (ClaC) neurons (green) and DAPI-stained nuclei (blue). Arrowhead points to an electrolytic lesion.

(F) Same brain as in (E), ~300 µm posterior to the tetrode tracks (left). Outlined region at higher magnification (middle) with ChR2-YFP (green) and tdTomato (red) in putative S1-projecting ClaC neurons. Putative S1-projecting ClaC neurons in the square shown at higher magnification (right).

(G) Example raster plots of responses during optogenetic stimulation. Optotagged (top, purple), Optomodulated (middle, cyan), or not influenced (bottom, blue).

Scale bars: 200 µm (E), 500 µm (F, left), 100 µm (F, middle) and 10 µm (F, right insets).

See also Figure S1.

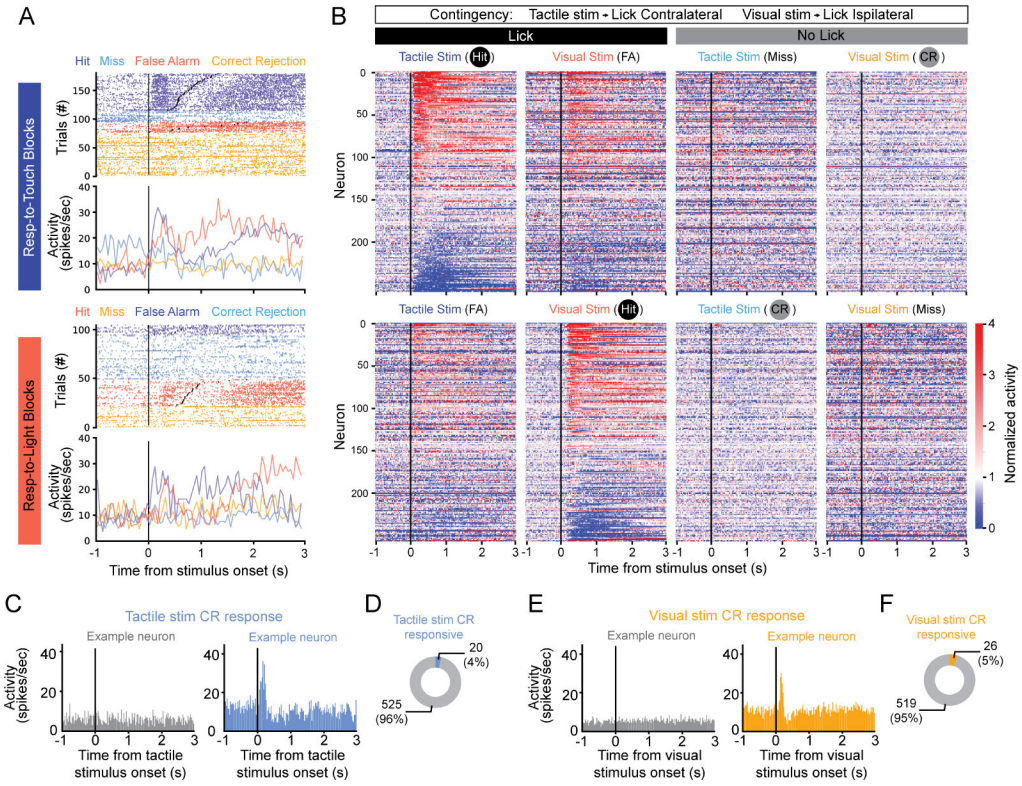

Figure 2. Few neurons in anterior claustrum exhibit sensory responses during Correct Rejection trials in a cross-modal selection task

(A) Raster plots and peristimulus time histograms (PSTHs) for example unit aligned to stimulus onset (black lines). Trials sorted by block type (top: Respond-to-Touch blocks, bottom: Respond-to-Light blocks). For each block type, trials are color-coded by stimulus-response pairing (Dark blue: tactile stimulus-lick; Light blue: tactile stimulus-no lick; Red: visual stimulus-lick; Orange: visual stimulus-no lick) and sorted by lick reaction time for Hit and False Alarm trials (Black dots: first lick).

(B) Heatmaps of mean stimulus-aligned activity, normalized to the unit's prestimulus baseline, for all claustrum neurons recorded in mice trained on touch→contralateral lick in Respond-to-Touch blocks and vision→ipsilateral lick in Respond-to-Light blocks (n = 247 units, 6 mice). Units sorted by mean activity during the 500 ms following stimulus presentation in Touch-Hit trials. Responses aligned to first lick shown in Figure S2A,B.

(C,E) PSTHs for Correct Rejection (CR) trials, when the mouse did not lick, for two example neurons showing no (left) or a significant (right) response to tactile (C) or visual (E) stimuli alone.

(D,F) Fraction of neurons significantly responding to tactile stimuli in CR trials in Respond-to-Light blocks (D) or visual stimuli in CR trials in Respond-to-Touch blocks (F, n = 9 mice), when mice did not lick.

See also Figure S2.

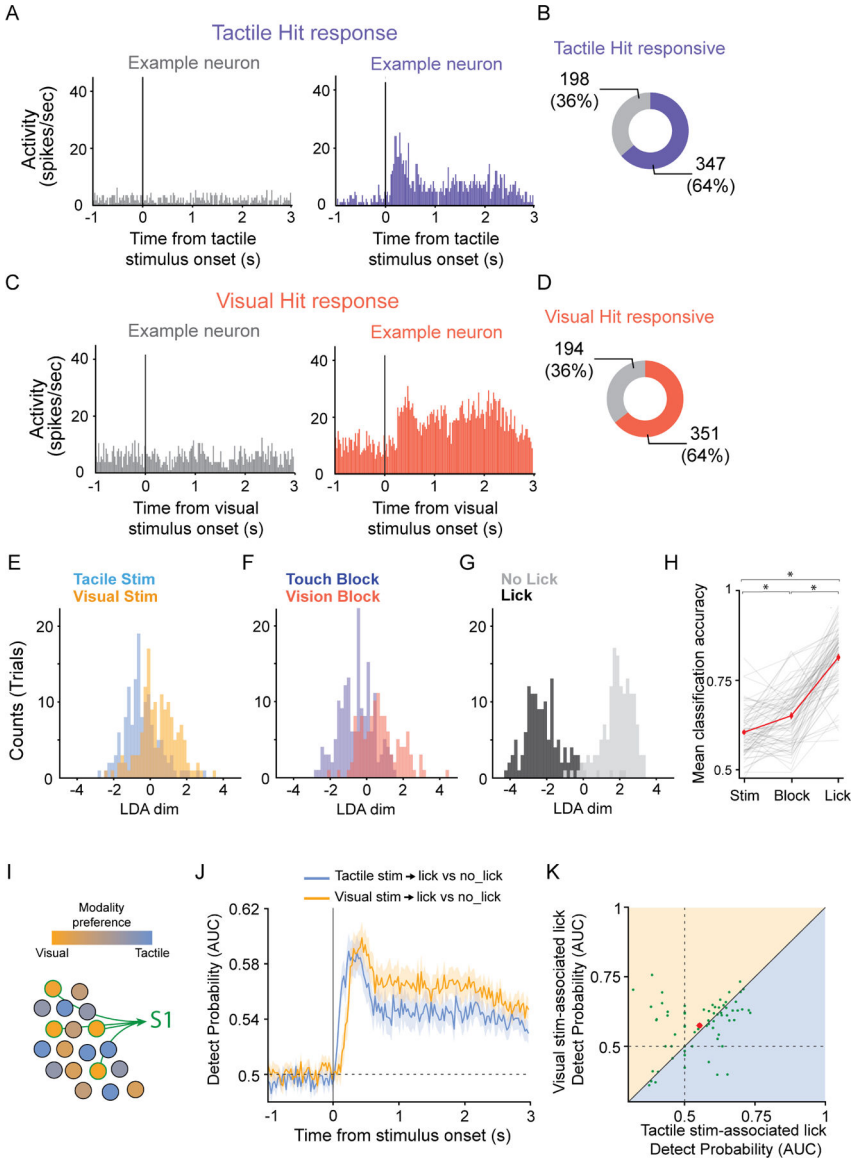

Figure 3. Claustrum neurons are recruited by movement

(A,C) Peristimulus time histograms (PSTHs) for two example claustrum neurons showing no (left) or a significant (right) response for Hit trials in Respond-to-Touch (A) or Respond-to-Light (C) blocks.

(B,D) Fraction of claustrum neurons significantly responding in Tactile-Hit trials (B) or Visual-Hit trials (D, n = 9 mice).

(E-G) Distribution of distances to the hyperplane from a linear discriminant analysis (LDA) on the responses from all trial types (Hits, Correct Rejections, Misses, and False Alarms) following stimulus presentation in an example behavioral session (n = 13 neurons) in which the LDA optimized separation by sensory stimulus presented (E, tactile versus visual), block type (F, Respond-to-Touch versus Respond-to-Light) or response type (G, lick versus no lick).

(H) Mean LDA classification accuracy for all behavioral sessions analyzed as in E-G (n = 73 sessions, 9 mice; mean: 7.5 neurons/session, range = 1 – 20). Grand averages shown in red ± SEM (Stimulus type: 0.60 ± 0.0074; Block type: 0.65 ± 0.0092; Response type (lick): 0.81 ± 0.0098; ANOVA p = 3.8e-42; Wilcoxon stim_v_block p = 3.9e-6; stim_v_lick p = 1.3e-13; block_v_lick p = 1.1e-12).

(I) Hypothesis: S1-projecting claustrocortical (ClaC) neurons preferentially respond during vision-associated licks, when mice suppress responses to tactile stimuli, regardless of the lick direction associated with the visual stimulus.

(J) Mean Detect Probability (DP, Area Under the ROC curve; AUC) for Tactile stim-associated lick versus no lick trials and Visual stim-associated lick versus no lick trials for putative S1-projecting ClaC neurons (n = 73 neurons, 9 mice). Shaded areas: standard errors.

(K) Scatter plot of the DPs for Visual stim-associated licks versus Tactile stim-associated licks for putative S1-projecting ClaC neurons (mean score for the 150 ms following DP onset; n = 73 neurons, 9 mice; Tactile stim-associated licks: 0.55 ± 0.012; Visual stim-associated licks: 0.57 ± 0.011; p = 0.28, Wilcoxon signed-rank test; mean: red dot ± SEM). See also Figures S2 and S3.

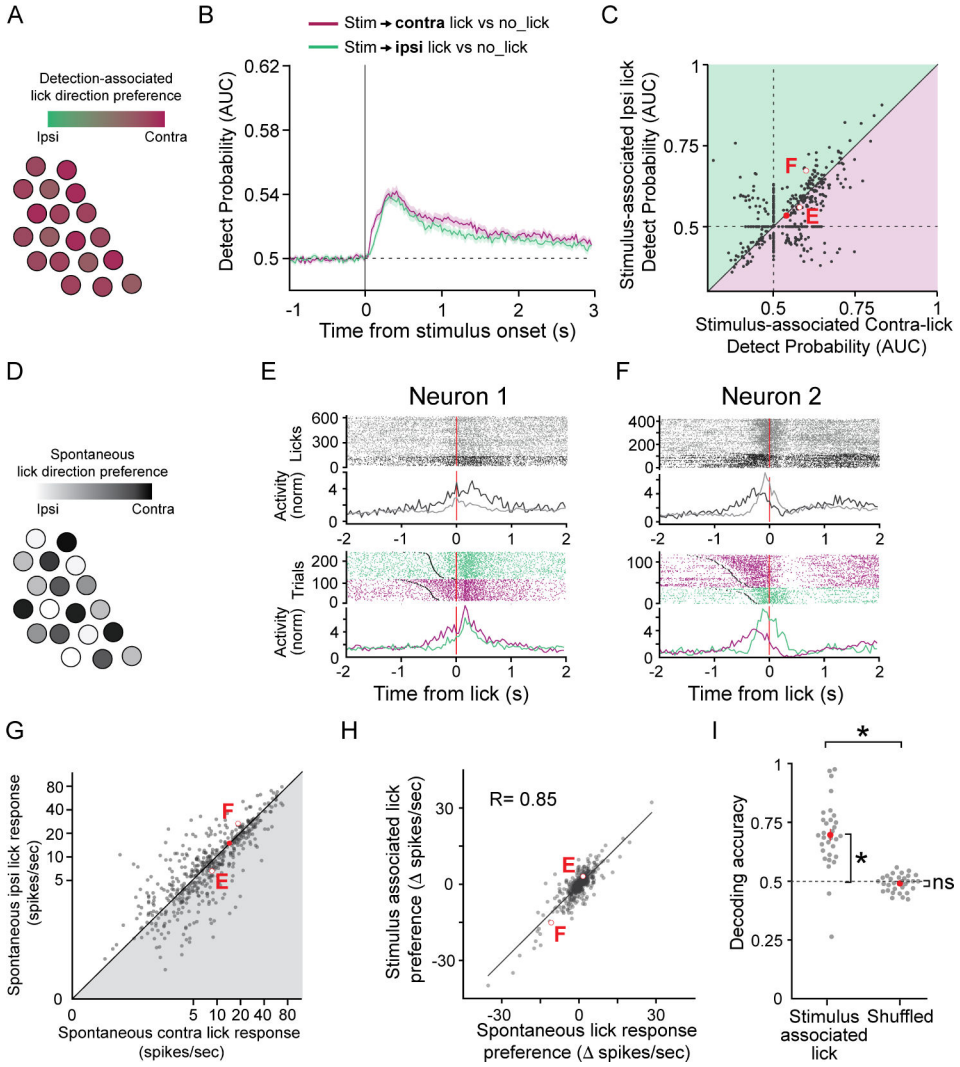

Figure 4. The activity of claustrum neurons is tuned to lick direction

(A) Hypothesis: Responses of claustrum neurons are biased for contralateral movement, regardless of sensory modality→lick direction association.

(B) Mean Detect Probability (DP) for lick versus no lick trials when the stimulus is associated with contralateral or ipsilateral licks (n = 545 neurons, 9 mice). Shaded areas: standard errors.

(C) Scatter plot showing the DPs for lick versus no lick trials when the stimulus is associated with contralateral or ipsilateral licks (mean score for the 150 ms following DP onset; n = 545 neurons, 9 mice; Ipsilateral Hits: 0.53 ± 0.0034; Contralateral Hits: 0.54 ± 0.0034; p = 0.060, Wilcoxon signed-rank test; mean shown: red dot ± SEM). Comparisons for example neurons in (E,F) shown with hollow red circles.

(D) Hypothesis: Claustrum neurons are individually tuned for lick direction, whether during reward-associated or spontaneous licks.

(E-F) Raster plots and PSTHs of the responses of two example neurons during spontaneous licks (ipsilateral: grey, contralateral: black) and Hit trials (ipsilateral: green, contralateral: purple) aligned to the first lick. Grey dots: stimulus onset during Hit trials.

(G) Scatter plot of individual claustrum neuron responses during spontaneous ipsilateral versus contralateral licks (n = 545 neurons, 9 mice). Mean: red; error bars (SEM) obscured by the symbol (Ipsilateral licks: 10.09 ± 0.52 spikes/sec; Contralateral licks: 10.15 ± 0.51 spikes/sec; p = 0.068; Wilcoxon signed-rank test). Comparisons for two example neurons in (E,F) shown with hollow red circles.

(H) Scatter plot and regression fit of the difference in response amplitudes for the two lick directions (Δ spikes/sec = response to contralateral − response to ipsilateral licks) during stimulus-associated versus spontaneous lick responses; ipsilateral preferring claustrum neurons have negative values (n = 545 neurons, 9 mice; p = 6.07e-156, Two-tailed Pearson's correlation test). Example neurons in (E, F) shown with hollow red circles.

(I) Performance of a maximum log-likelihood decoder tuned on spontaneous lick responses used to predict stimulus-associated lick direction (n = 31 sessions, 6 mice, range 6–15 neurons; Decoder: 0.69 ± 0.024 versus Chance: 0.5, p = 8.6e-6; Shuffled: 0.49 ± 0.0060 versus Chance: p = 0.20; Decoder versus Shuffled: p = 7.2e-6, Wilcoxon signed-rank test). Each grey point: a session; red dots: mean ± SEM; dashed black line: chance level.

See also Figures S4 and S5.

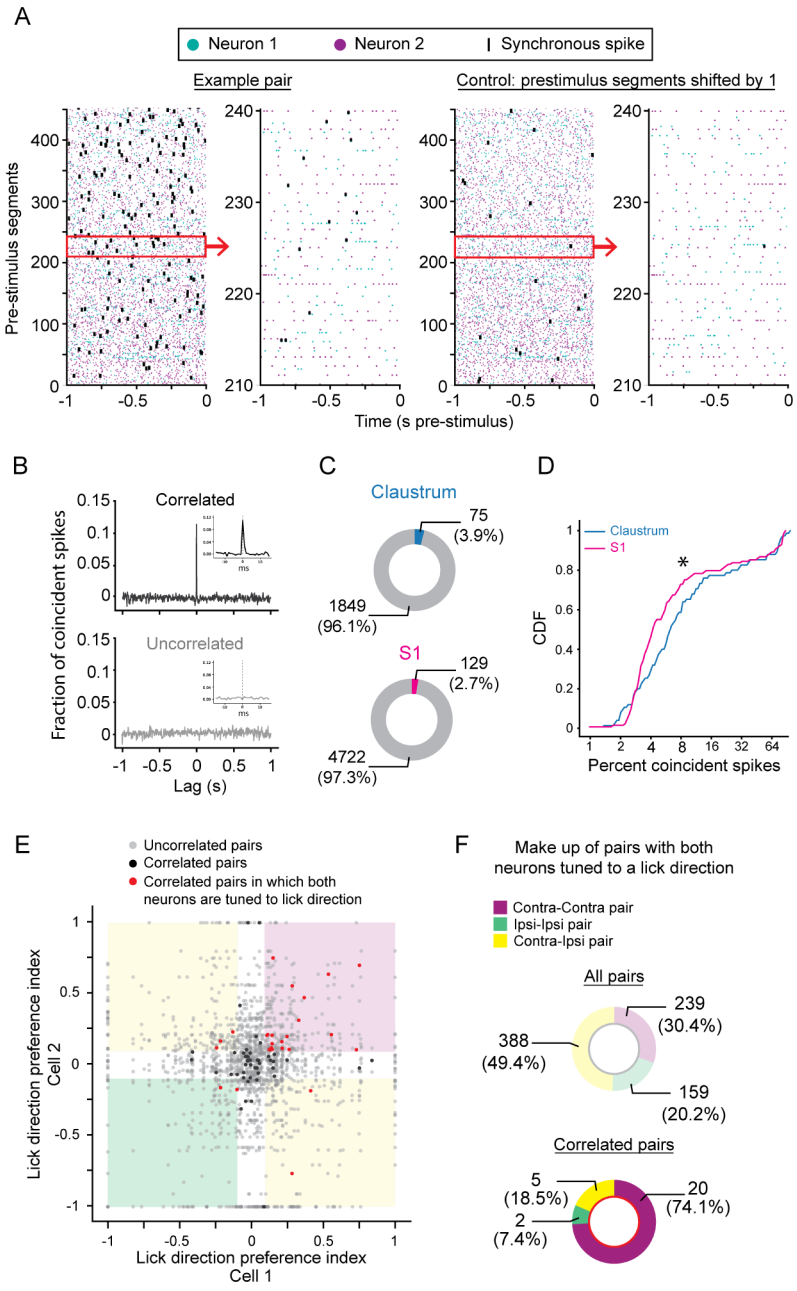

Figure 5. Claustrum neurons preferring contralateral licks exhibit synchronous activity

(A) Raster plots showing spike times during the 1 s prior to stimulus presentation for two simultaneously recorded claustrum neurons (far left, neuron 1: teal, neuron 2: purple). Synchronous spikes marked in black. Control raster plots (right) with the prestimulus segments from neuron 2 shifted by 1 segment. Subsets of the prestimulus and control segments outlined by the red boxes shown in more detail (left, far right).

(B) Example crosscorrelograms (CCGs) for pairs of claustrum neurons showing significantly correlated (top) and uncorrelated (bottom) activity. Insets show magnified, unfiltered CCGs. **(C)** Proportion of pairs exhibiting significantly correlated activity in claustrum (top, N = 9 mice) and S1 (bottom; N = 4 mice; p = 0.0090, Chi-Square test).

(D) Cumulative distribution of the percentage of coincident spikes for pairs of significantly correlated claustrum (blue line; n = 75 pairs, 9 mice) and S1 neurons (magenta line; n = 129 pairs, 4 mice; Claustrum: 7.2 ± 1.2% coincident spikes, S1: 6.3 ± 0.87% coincident spikes, SEM; p = 0.042, Mann-Whitney U test). Note the x-axis is log2 scaled.
(E) Scatter plot of the Lick Direction Preference Index (LDPI) for each pair of claustrum neurons tested. Red dots: significantly correlated pairs composed of two neurons with LDPI absolute values greater than 0.1. Black dots: significantly correlated pairs with one or both neurons with a LDPI absolute value less than 0.1. Grey dots: uncorrelated pairs. White regions indicate 0.1 cutoff of the LDPI. Pink region: pairs both prefer contralateral licks; green region: pairs both prefer ipsilateral licks; yellow regions: pairs with different lick direction preferences.
(F) Lick direction preferences for all recorded pairs with strong lick direction preferences (top, Purple: contra-contra; Green: ipsi-ipsi; Yellow: contra-ipsi). Lick direction preferences for all significantly correlated pairs with strong lick direction preferences (bottom), showing enrichment for pairs with concordant contra-contra lick direction preferences (p = 3.38e-6; Chi Square test).
See also Figure S6.

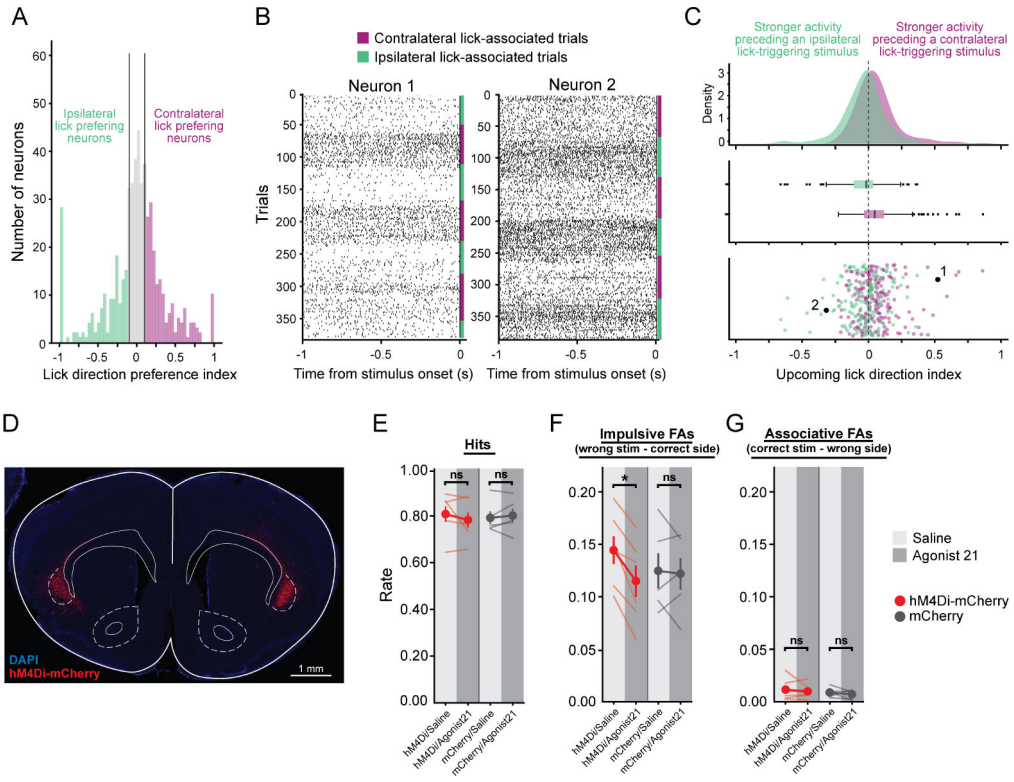

Figure 6. Claustrum neurons encode lick direction prior to stimulus onset and contribute to the control of impulsive licks in the task

(A) Lick Direction Preference Index (LDPI) for all recorded claustrum neurons (Purple: n = 192 neurons with contralateral-lick preferences, LDPI cut-off 0.1; Green: n = 163 neurons with ipsilateral-lick preferences, LDPI cut-off −0.1).

(B) Raster plots for two claustrum neurons with shifts in baseline firing prior to stimulus onset.

(C) Distribution of an Upcoming Lick Direction Index (ULDI), calculated using pre-stimulus firing rates, for neurons preferring contralateral licks (purple, 0.062 ± 0.012 (SEM), n = 192 neurons, 9 mice, contra_v_0 p = 2.7e-6, Wilcoxon rank-sum test) or ipsilateral licks (green, −0.040 ± 0.012, n = 163 neurons, 9 mice, ipsi_v_0 p = 0.0029, Wilcoxon rank-sum test; contra_v_ipsi p = 3.2e-8, Mann-Whitney U test). Results were similar following removal of outliers with absolute z-scored ULDIs greater than 3 SD of the mean (contralateral preferring: n = 188, 4 outliers removed, 0.048 ± 0.0097; ipsilateral preferring: n = 160, 3 outliers removed, −0.0288 ± 0.011; Paired t-test contra_v_0 p = 1.7e-6; ipsi_v_0 p = 0.0089; Independent samples t-test contra_v_ipsi p = 2.3e-7; Cousineau and Chartier, 2010).

(D) hM4Di-mCherry expression (red) in claustrocortical (ClaC) neurons in a coronal section from a mouse used in the behavioral experiments reported in E-G.

(E-G) Hit (E), Impulsive False Alarm (F) and Associative False Alarm (G) rates for mice with ClaC neurons expressing hM4Di-mCherry (red points, n = 6 mice) or mCherry only (grey points, n = 5 mice). The overall Hit rate (E, mixed ANOVA with repeated measure for injection and independence for virus: interaction of virus and injection F = 1.5; p = 0.25), Impulsive FAs rate in which mice lick the correct reward port for that block but in

response to the incorrect sensory stimulus (F, mixed ANOVA with repeated measure for injection and independence for virus: interaction of virus and injection F = 6.1; p = 0.036, post hoc paired-test: hM4Di-Saline vs hM4Di-Agonist21 p = 4.40e-3; mCherry-Saline vs mCherry-Agonist21 p = 0.795) and Associative FA rate in which mice lick the incorrect port for that block type (G, mixed ANOVA with repeated measure for injection and independence for virus: interaction of virus and injection F = 0.0; p = 0.99) are shown. Light lines: mean Hit and FA rates for individual mice for days when they received DREADD agonist (dark grey bars) or vehicle (light grey bars).

See also Figure S7.

Key resources table

REAGENT or RESOURCE	SOURCE	IDENTIFIER
Antibodies		
Rabbit anti-DsRed polyclonal antibody	Living Colors, Clontech Laboratories	RRID: AB_10013483
Chicken anti-GFP antibody	Aves	GFP-1020, RRID:AB_10000240
Alexa Fluor 488 AffiniPure donkey anti-chicken IgY (IgG) (H+L) antibody	Jackson ImmunoResearch Laboratories Inc	703–545-155, RRID:AB_2340375
Rabbit anti-parvalbumin antibody	Swant	PV27, RRID: AB_2631173
Monoclonal mouse anti-parvalbumin antibody	Sigma-Aldrich	P3088, RRID: AB_477329
DyLight 405-AffiniPure donkey anti-mouse IgG (H+L) antibody	Jackson ImmunoResearch Laboratories Inc	715–475-150, RRID: AB_2340839
Alexa Fluor 594 donkey anti-rabbit IgG (H+L) Highly Cross-Adsorbed Secondary Antibody	ThermoFisher (Invitrogen)	A-21207, RRID: AB_141637
AlexaFluor 647-conjugated donkey anti-rabbit antibody	Jackson ImmunoResearch Laboratories Inc	711–606–152, RRID: AB_2340625
Bacterial and virus strains		
rAAV2-retro-Syn-Cre	Tervo et al., 2016	HHMI - Janelia research campus
AAVrg-pmSyn1-EBFP-Cre	Madisen et al., 2015	Hongkui Zeng: Addgene viral prep #51507-AAVrg
AAVrg.hSyn.HI.eGFP-Cre.WPRE.SV40	Gift from James M. Wilson	James M. Wilson: Addgene viral prep #105540-AAVrg
AAV5-hSyn-DIO-hM4D(Gi)-mCherry	Krashes et al., 2011	Bryan Roth: Addgene viral prep #44362-AAV5
AAV5-hSyn-DIO-mCherry	Gift from Bryan Roth	Bryan Roth: Addgene viral prep #50459-AAV5
AAV5-EF1a-DIO-hChR2(H134R)-EYFP-WPRE-HGH	Gift from Karl Deisseroth	Karl Deisseroth: Addgene viral prep #20298-AAV5
AAV-DJ-CamKIIa-hChR2(H134R)-eYFP	Gift from Karl Deisseroth	Stanford Gene Vector and Virus Core, GVVC-AAV-36
Chemicals, peptides, and recombinant proteins		
Red retrobeads	Lumafluor	*Red Retrobeads*
Cholera Toxin Subunit B (Recombinant), Alexa Fluor™ 555 Conjugate	ThermoFisher Scientific	C34776
DREADD agonist 21 dihydrochloride	Tocris	6422
Experimental models: Organisms/strains		
Mouse: Ai9, Ai14, C57BL/6J, CD1	The Jackson Laboratory; Charles River	007909, 007914 and 000664
Software and algorithms		
Python		3
Matlab	Mathworks	2019
Image J	Schneider et al., 2012	https://imagej.nih.gov/ij/
Code for analysis and figure generation	This paper	DOI: 10.5281/zenodo.5655393